**Characterisation and Optimisation of AZO Thin Films Fabricated by Sol-Gel Methods**

**By Weite Gu (N)**
Fourth-year undergraduate project
in Group B, 2014/2015

I hereby declare that, except where specifically indicated, the work submitted herein is my own original work.

Signature: _____ Date: 27 May 2015

# Technical Abstract

**Characterisation and Optimisation of AZO Thin Films Fabricated by Sol-gel Methods**

*By Weite Gu (Newnham College)*

With the growing market for touchscreen devices, light emitting diodes and photovoltaic cells, transparent conductors are becoming increasingly in demand. The current industrial standard material is indium tin oxide (ITO). It has an excellent electrical conductivity and a high optical transmittance, both of which are important performance indicators for applications as transparent electrodes.

However, ITO has a critical drawback due to indium's scarcity and cost. Hence, there has been substantial interest in finding a suitable and sustainable alternative material to replace ITO before it becomes prohibitively expensive. Zinc oxide (ZnO) is an extremely attractive replacement for ITO due to its natural abundance. ZnO can be made highly conductive through degenerate doping using dopants such as aluminium. This project focuses on producing thin films of ZnO doped with aluminium, a material commonly known as AZO.

While AZO would already enable marked cost-saving compared to ITO due to low cost of raw materials, a real game-changing technology would be the sol-gel fabrication technique. This is a solution-processable technique that avoids the need for vacuum, and thus can be achieved with a much lower cost and complexity. This project explores sol-gel AZO synthesis and AZO deposition via spin-coating. Sputter-coated films were also fabricated to act as a benchmark for the spin-coated films.

A commercial AZO dispersion was purchased to spin-coat onto glass substrates, but films made from this solution exhibited very poor electrical conductivity. To improve the quality of the solution, AZO was synthesised via reflux. Zinc acetate was used as the Zn precursor, while two types of aluminium precursors were used. Films made from the synthesised solutions showed a marked improvement in conductivity compared to films made from the commercial solution. Between the two aluminium pre-

cursors, aluminium nitrate produced AZO films with superior electrical properties.

Next, multi-layer coating was explored as a way to improve film quality by reducing voids in the film. It was shown that conductivity increased with increasing number of layers up to three layers. After which, film quality starts to degrade, possibly due to repeated cycles of heating and cooling between coatings.

Drying parameters were then investigated. Drying was defined as a short period of heating between coatings, at a moderate temperature. A drying temperature of 300 °C and a drying duration of two minutes were found to be appropriate in this project. Dendritic solidification was observed in some films, but the exact reason was unknown.

After a basic set of synthesis and deposition parameters was determined, the focus shifted to investigating the effect of AZO doping concentrations. Solutions with doping levels ranging from 0 wt% to 2 wt% were synthesised. Generally, the sheet resistance of the films decreased with increased doping, until a minimum was reached at 1 wt% doping. Optical transmittance did not seem to be affected by the doping level, but Tauc gap increased with doping as expected. At a nominal doping concentration of 2 wt%, the Tauc gap was deduced to be 3.341 eV.

The annealing temperature and duration were then investigated. Both conductivity and optical transmittance improved at higher annealing temperatures. AZO films annealed at 500 °C had the best performance. The annealing duration was varied at 30, 60 and 90 minutes, but it did not show a significant influence on film performance. Attempts were also made to improve film performance by coating AZO over graphene, and by incorporating carbon nanotubes into AZO solution. The latter approach achieved modest success.

In conclusion, sol-gel deposited AZO is a promising replacement of ITO. While the results are encouraging, much research is still needed to develop a solution-processable technique that is highly repeatable.

# Contents

# 1 Symbols and Abbreviations

| | |
|---|---|
| $\omega$ | Spin speed in revolutions per minute |
| AFM | Atomic force microscopy |
| AZO | Aluminium doped zinc oxide |
| CNT | Carbon nanotube |
| $d$ | Film thickness |
| EDX | Energy dispersive X-ray spectroscopy |
| FOM or $\phi$ | Figure of merit |
| ITO | Indium tin oxide |
| MEA | Monoethanolamine |
| MWCNT | Multi-wall carbon nanotube |
| PVD | Physical vapour deposition |
| RF | Radio frequency |
| SEM | Scanning electron microscopy |
| $T$ | Percentage transmittance |
| TCO | Transparent conductive oxide |
| TEM | Transmission Electron Microscopy |
| VDP | Van der Pauw method for resistance measurement |
| XRD | X-ray diffraction |

# 2 Acknowledgement

I would like to thank Ammar, Akmal, David, Jonathan, Jong, Kham, Malik, Sarwat and Shane for showing me the ropes of various equipment and experimental techniques. I am also grateful to Shane for providing the AZO target for sputter coating, Jack for providing the graphene films and Matt for providing the MWCNT solution. Sincere appreciation goes to Dr Durkan for his help on AFM, and Dr Flewitt and Professor Wilkinson for granting me access to their research facilities. Further thanks go to Yury and Myriam for their kindness when the original wet lab I worked in had an unanticipated long-term closure. I also wish to thank my Director of Studies, Dr Claire Barlow, for her continuous guidance and support. Finally, I wish to express my heartfelt appreciation for my supervisor Dr Hannah Joyce. Thank you for sharing your wisdom with me, not just on research, but also on life.

# 3 Introduction and Motivation

## 3.1 Transparent Conductive Oxides

Transparent conductive oxides (TCOs), as the name suggests, are optically transparent and electrically conductive oxides. They form important components in many electronic devices such as photo-voltaic cells, light emitting diodes, displays, touchscreens and gas sensors. They are usually deposited as thin films so as to serve as windows for light to pass through to the active materials beneath (e.g. where carrier generation occurs). They can also function as ohmic contacts for carrier transport into and out of the active materials. It is desirable for TCOs to have a wide bandgap ($\geq 3.2\,\text{eV}$) such that most light from the solar spectrum can pass through the TCO films instead of being absorbed by them. The current industrial standard TCOs are primarily n-type semiconductors as p-type TCOs exhibit much lower carrier mobilities due to the large hole effective masses of these materials [1].

The current TCO that is widely used in electronic devices is indium tin oxide (ITO). It can be found in most touchscreen devices such as mobile phones. ITO's sheet resistances can be as low as $10\,\Omega/\text{sq}$ in high quality commercial products [2]. Its optical transmittance in the visible range is easily above 85%. ITO also has stable mechanical properties and can survive in a solar cell for 25 to 30 years on a rooftop [3].

However, despite ITO's superior performance, indium is an expensive material and is harmful to both humans and the environment [4]. Also, the scarcity of indium is becoming a problem. The US Geographical Survey projected that indium mines might become depleted in 2020 [5]. Therefore, alternative materials are urgently needed to replace ITO in its various applications. The candidate materials include highly doped zinc oxide (ZnO), graphene and carbon nanotube (CNT) thin films. A high degree of complexity is involved in the making of graphene and CNTs, so low cost mass production is not yet practical. In contrast, ZnO can be synthesised easily in large quantities, and the required materials are commonly available and inexpensive. Hence, much attention is being paid to zinc oxide as a promising replacement of ITO due to its abundance and comparable material properties.

## 3.2 Doped Zinc Oxide as a Promising TCO

The undoped ZnO shows an n-type conductivity due to the existence of native defects [6], and has a wide band gap of about 3.37 eV [7]. However, the conductivity of this undoped ZnO is thermally unstable, so doping ZnO with Group III ions is necessary to generate extra electrons [6][8]. While gallium and indium can also be used, aluminium has been the most promising dopant due to its comparable ionic radius to $Zn^{2+}$ and low material cost. The resulting material is known as aluminium doped ZnO, or simply AZO. The doping of ZnO is substitutional as $Al^{3+}$ ions replace $Zn^{2+}$ ions in ZnO lattice. Each ionised Al atom contributes one extra valence electron as a mobile charge carrier, so Al doping improves the electrical conductivity of the material considerably [9]. While doping ZnO with a suitable amount of Al can increase its material properties notably, excessive doping could adversely affect carrier mobility due to ionised impurity scattering [10][11]. Hence, one issue explored in this project was to determine the ideal doping concentration of AZO.

# 4 Design of Experiments

## 4.1 Deposition Techniques

Besides the focus on improving the material properties through doping, much research has been conducted on the various thin film deposition methods, as they too have a great impact on the performance and cost-effectiveness of the fabricated thin films.

### 4.1.1 Sputter Deposition

Sputter deposition is a physical vapour deposition (PVD) method of thin film deposition based on momentum transfer. A weakly ionised argon plasma is generated and used to bombard the AZO target. Some atoms are knocked off from the target and deposited onto the substrate. The mean free path of atoms is smaller than the size of the sputtering chamber. Frequent collisions are needed to ensure a good step coverage and film uniformity [12]. A schematic of this technique is shown in Figure 1.

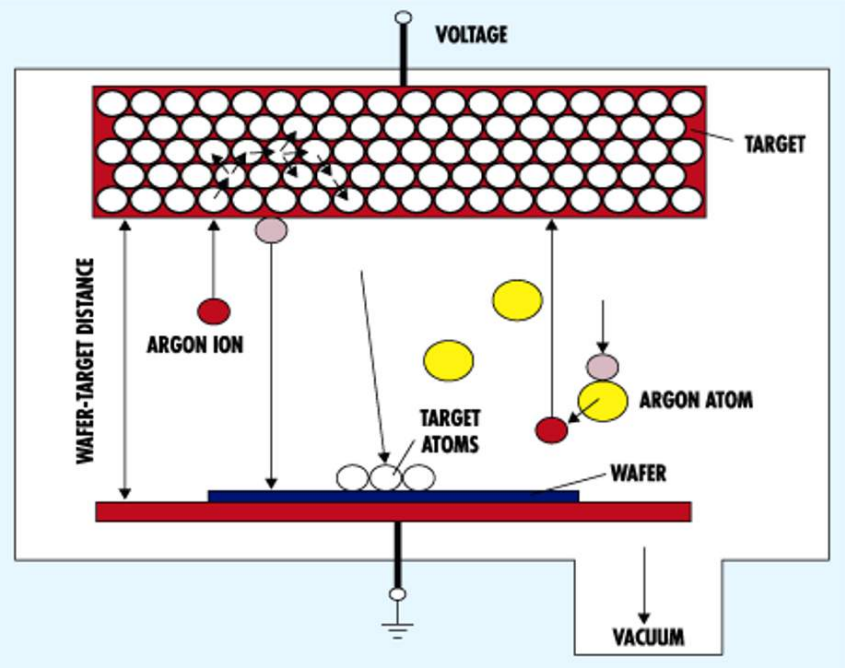


Figure 1: A schematic of sputter deposition. Source: Edited from micromagazine.org [13]

This is a popular method in TCO deposition as it has consistently produced AZO films with sheet resistances as low as $13\,\Omega/\text{sq}$ and optical transmittances as high as 85% across the visible spectrum of wavelengths [14]. However, the disadvantages of this method are the need for vacuum condition (typically 10 - 100 mTorr) and its low deposition rate ($< 1\,\text{nm/s}$). Also, once the sputter targets have been made, making additional modifications to them such as the addition of new dopants cannot be easily done.

### 4.1.2 Sol-Gel Process

The sol-gel process is a low-temperature process that uses inorganic or metal organic precursors to produce metal oxide molecules in solution form. The solution is synthesised based on the hydrolysis and condensation reactions of organometallic compounds in alcohol-based solutions. Several methods can then be used to deposit AZO films using the solutions, two of which will be discussed below.

**Spin-Coating** For this technique, the material to be deposited is dissolved or dispersed into a solvent, and this coating solution is then deposited onto the substrate surface and spun off to leave a uniform layer of thin film on the substrate. As shown

in Figure 2, the four key phases in the spin-coating process are:

1. Deposition of solution onto the substrate.
2. Spreading of solution from centre of substrate to the sides (spin-up).
3. Gradual thinning of solution (spin-off).
4. Gelation due to solvent evaporation.

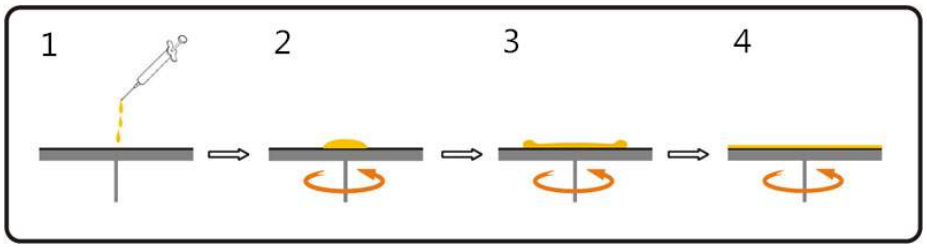


Figure 2: A schematic of spin-coat deposition. Source: Edited from globalspec.com [15].

As the deposited film is thinned by the centrifugal draining, it tends to be uniform since a balance occurs between the radially outward centrifugal force and the radially inward viscous force. Even with non-planar substrates, very homogeneous film thicknesses can be achieved.

**Dip-Coating** For this technique, the substrate to be coated is immersed in the solution and then withdrawn at a well-defined speed under controlled temperature and atmospheric conditions. A schematic is shown in Figure 3. In order to have a uniform film thickness, vibration-free mountings and smooth movement of the substrate are essential. Compared to spin-coating, dip-coating requires more sophisticated equipment.

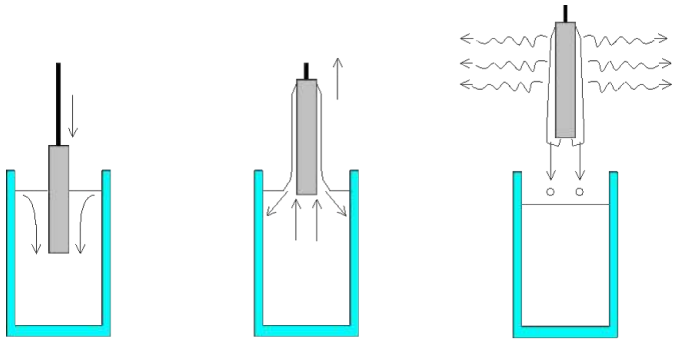

Figure 3: A schematic of dip-coat deposition. The three phases of this technique are substrate dipping, wet layer formation and solvent evaporation. Source: Sol-gel.com [16].

### 4.1.3 Advantages and Disadvantages of the Sol-Gel Technique

Being a solution processable technique, sol-gel coatings offer many advantages for the fabrication of thin films over other techniques. These include 1) Excellent control of the purity and stoichiometry of the coating solutions. 2) Ease of compositional modifications. 3) Suitability for deposition on large area substrates. 4) Simple and inexpensive equipment [17] [18].

Its disadvantage is that the sheet resistance of the films produced is usually at least one order of magnitude higher than that of the sputter-coated films [17]. One possible reason is that there are many more parameters which need to be optimised in sol-gel processes. Choice of precursors, number of layers deposited, drying temperature, annealing temperature and atmosphere could all play an important role in shaping the properties of the deposited thin films. Also, as sol-gel procedures are much more manual, good quality films are less reproducible than sputter-coated ones. However, by going through careful optimisation and process control, this technique shows enormous potential in becoming the preferred low cost deposition method of the future [19].

## 4.2 Research Methodology and Goals

In order to produce AZO thin films of excellent electrical and optical properties, various processes of spin-coating were optimised. This technique was chosen as opposed to dip-coating due to the availability of high quality spin-coating equipment. The goal was to produce films with a sheet resistance of lower than 147 $\Omega$/sq. Up to now, this

is the lowest value reported in literature by using the spin-coating technique [20]. The target optical transmittance over the wavelength spectrum of 400 nm to 900 nm was 85% and above. Sputter-coated films were also produced and characterised to act as a performance benchmark for the spin-coated films. The ultimate goal was to devise a low cost, flexible and solution-processable way of producing transparent and conductive AZO thin films.

# 5 Film Deposition Procedures

## 5.1 Sputtering

Sputter-coated samples were made using a radio frequency (RF) magnetron system. The chamber was evacuated to a base pressure of $3 \times 10^{-6}$ mbar. Sputtering was carried out at a pressure of $7.3 \times 10^{-3}$ mbar in pure argon gas with an RF power of 75 W. 2 cm×2 cm Corning glass substrates were placed 10 cm from the target. The target was made of ZnO powder doped with 1 wt% of $Al_2O_3$.

## 5.2 Spin-Coating

### 5.2.1 Solution Synthesis

Several types of solutions were used as starting solutions for thin film deposition in order to draw conclusions on which aluminium precursor works better and what is the ideal doping concentration.

Firstly, an AZO solution was purchased from US Research Nanomaterials. This solution contained zinc oxide nanoparticles doped with 2 wt% of $Al_2O_3$ in a water dispersion. The original concentration was 3 M. Some of it was diluted to 0.75 M and 1.5 M by adding in more distilled water. The purchased water-based dispersion produced poor quality films, as will be discussed in further detail in Secion 7. For this reason, more solutions were synthesised in-house, as discussed below.

AZO solutions of 0.25 wt% 0.5 wt%, 1 wt% and 2 wt% doping were synthesised in the wet lab. A ZnO solution with no doping was also produced to investigate the effectiveness of doping. Solid aluminium chloride hexahydrate ($AlCl_3 \cdot 6\,H_2O$) and aluminium nitrate nonahydrate ($Al(NO_3)_3 \cdot 9\,H_2O$) were used as dopant precursors in

the synthesis of AZO solutions. The synthesis steps developed in this project are as follows:

1. Dissolve 2.725 g of zinc acetate dihydrate ($Zn(CH_3COO)_2 \cdot 2\,H_2O$) in 30 ml of ethanol.
2. Add monoethanolamine (MEA) drop by drop until MEA and Zn reach a molar ratio of 1:1. Stir at room temperature until the solution becomes clear and homogeneous.
3. Dissolve an appropriate mass of the aluminum precursors, depending on the desired doping level, in 10 ml of ethanol. Stir at room temperature until the solution becomes clear and homogeneous.
4. Mix both solutions together and reflux for three hours at 80 °C, under constant magnetic stirring.
5. Leave the solution to age under room temperature for 24 hours.

The chemical reaction happens in two steps.

1. Hydrolysis: $Zn(CH_3COO)_2 + 2\,H_2O \longrightarrow Zn(OH)_2 + 2\,[(CH_3COO)OH]$

2. Condensation: $Zn(OH)_2 \longrightarrow ZnO + H_2O$

Overall: $Zn(CH_3COO)_2 + 2\,H_2O \longrightarrow ZnO + 2\,[(CH_3COO)OH]$

In this reaction, MEA acts as a stabilizer and helps to yield a clear and homogeneous solution [21]. The concentration of Zn in the synthesized solutions was kept at 0.3 M. Ethanol was chosen as the solvent because zinc acetate has a higher solubility of 750 g/litre in it than in other organic solvents [22]. Methanol was also trialled instead of ethanol, but the results were unsatisfactory due to low solubility of zinc acetate in methanol. As mentioned earlier, two different aluminium precursors were used, namely $Al(NO_3)_3$ and $AlCl_3$. By doing this, a comparison can be made on which precursor enables better films to be fabricated. However, $AlCl_3$ may be a less practical option as its price is about five times that of $Al(NO_3)_3$ [23]. The reflux set-up is shown in Figure 4.

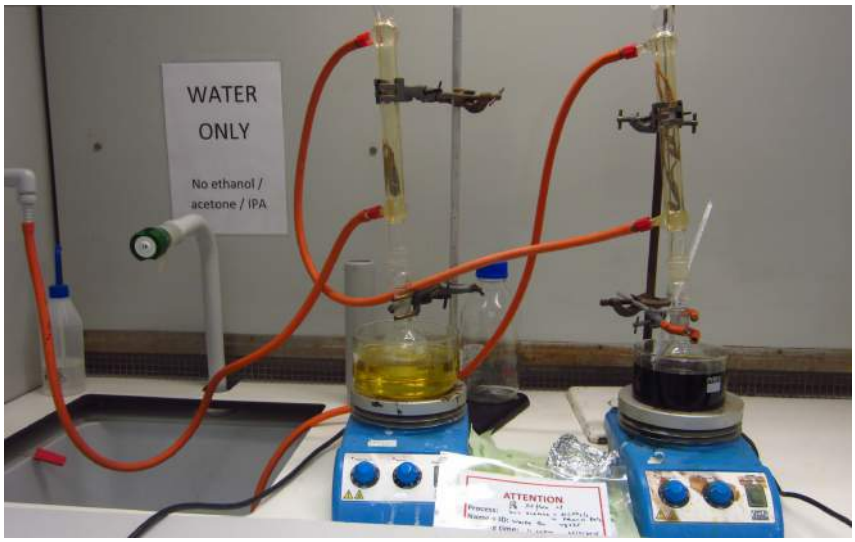


Figure 4: Experimental set-up for refluxing AZO solutions.

### 5.2.2 Film Preparation

2 cm×2 cm Corning glass substrates were cleaned in isopropanol and acetone in an ultrasonic bath for five minutes each. Oxygen plasma cleaning was done for five minutes on some substrates using a Diener etcher but this was discontinued as it did not make a noticeable difference on the the properties of films. For spin-coating, a Laurell WS-400 spin coater was used. With a pipette, the solution was manually deposited onto the substrate before it was set to spin. For preliminary experiments, procedural parameters were varied to determine the best experimental practice. One water-based and two ethanol-based coating solutions were used to study the effect that base solution and aluminium precursors have on film properties.

After a good set of basic procedures was established, subsequent experiments focused on determining the effect that doping concentration, annealing temperature and annealing duration have on film properties. The fabrication parameters for both sets of experiments are summarised in Table 1.

| **Parameters** | **Preliminary Samples** | **Subsequent Samples** |
|---|---|---|
| Spin speed (rpm) | 1000 - 3000 | 2000 |
| Solution concentration (molar) | 0.75 - 3 | 0.3 |
| Spin duration (s) | 15 - 60 | 25 |
| No. of coatings | 1 - 6 | 3 |
| Drying temperature (°C) | 100 - 300 | 300 |
| Drying duration (min) | 1 - 10 | 2 |
| Doping concentration of ZnO (wt %) | 2 | 0 - 2 |
| Annealing temperature (°C) | 300 | 300 - 500 |
| Annealing duration (min) | 60 | 30 - 90 |
| Base solution | Water, ethanol | Ethanol |
| Aluminium precursor | $Al(NO_3)_3$, $AlCl_3$ | $Al(NO_3)_3$ |

Table 1: A summary of the spin-coat parameters for both sets of samples.

For each set of fabrication parameters under the column "subsequent samples", two identical films were made and characterised on the same equipment. This was done to investigate the reproducibility of the spin-coating technique developed.

# 6 Characterisation Techniques

## 6.1 Particle Size Measurement

A Malvern Zetasizer was used to measure the size of nanoparticles in AZO and ZnO solutions. The refractive index of AZO was taken to be 2.675 and that of the undoped ZnO was taken to be 2.054 [24].

## 6.2 Profilometry

A Dektak 200-Si profilometer was used to determine the thicknesses of the films in early stages of this project. Kapton tape was used to mask a section of the substrate before the solution was spun on it. The tape was peeled off during drying and annealing to avoid the charring of tape. This did not prove to be an accurate method of determining film thicknesses, as even after the tape was peeled off, some adhesive materials with a significant thickness (about 50 nm) was left on the substrates. Also,

this Dektak operated very slowly and broke down often. Hence it was only used to determine the relationship between spin speed and film thickness. The thicknesses of the films made in later stages were estimated by looking at film cross-sections using a scanning electron microscope (SEM).

## 6.3 Van der Pauw Sheet Resistance Measurement

The sheet resistances of AZO films were determined using the Van der Pauw (VDP) method on a Keithley-4200 semiconductor characterisation system. This involved applying currents and measuring voltages using four small contacts placed in a square configuration on the film surface. The working principle of this method is shown in Figure 5. A set amount of current ranging from 1 nA to 100 nA was forced through two terminals while the voltage across them was measured. This was done eight times to cover all possible combination of probes and directions of current flow. This is an easy and relatively accurate way of deducing the sheet resistance of thin films.

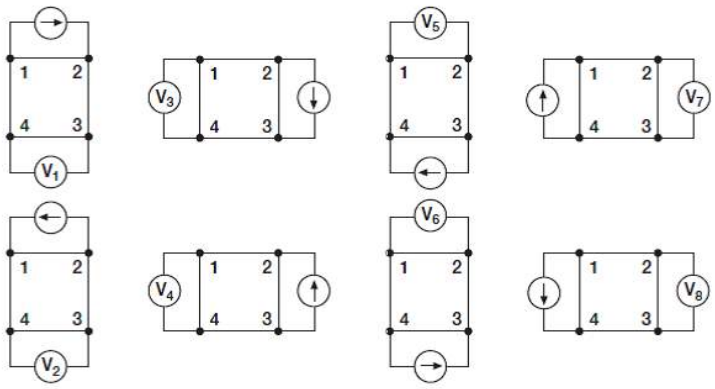


Figure 5: Configuration of probes for VDP measurement. Source: Keithley application notes [25].

In this project, silver paste was deposited on the perimeter of the film to form ohmic contacts between the film and the probes, as shown in Figure 6. Eight contacts were made so that readings could be taken from two different square formations. For each formation, two readings were taken. Since there were two films made under the same parameters, eight readings were obtained for films made with each set of fabrication parameters. Every sheet resistance value presented in the Results and Discussions section is therefore an average of eight readings, with the error bars covering the maximum and minimum readings out of the eight readings.

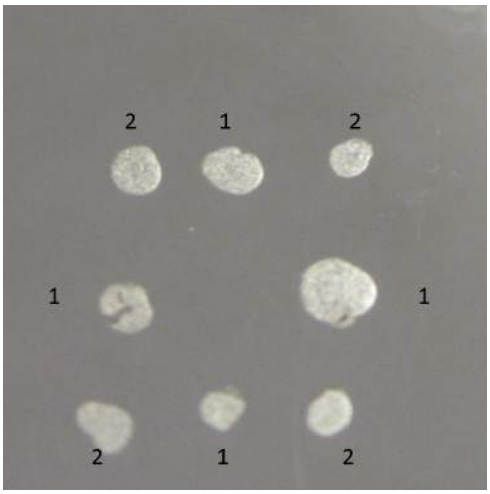


Figure 6: Silver contacts placed in a 1cm by 1 cm square on sample surface.

## 6.4 UV-Visible Spectroscopy

The transmittance of films was measured using a Unicam UV-Visible spectrometer. Light of wavelengths ranging from 300 nm to 1000 nm was passed through the samples and transmittance data was collected at 2 nm intervals.

## 6.5 Optical Microscopy, SEM, EDX and AFM

A Nikon Eclipse optical microscope was used to perform a preliminary study of the film surface.

A Leo Gemini 1530VP SEM was used to study the morphology of the film surface in detail. Accelerating voltages from 3 kV to 12 kV were used and secondary electrons ejected from the film surface were collected to produce images. As the samples were themselves conductive, prior sputtering of conductive material was not required.

An energy dispersive X-ray spectrometer (EDX) housed within the SEM chamber was used for the fingerprinting of elemental composition on film surfaces. An accelerating voltage of 15 kV was used. The incident beam excites electrons in inner shells of the elements, ejecting them from the shells while creating empty orbitals, which will be filled up by electrons from outer, higher-energy shells. The energy released from this relaxation is radiated as X-ray photons, whose wavelengths are characteristic of the element. The number of photons collected corresponds to the concentration of that

particular element in the area of the scan. This allows the elemental composition of the specimen to be measured. This is a suitable technique for the AZO films as the elements of interest all have an atomic number $\geq 6$. Thus the energies of the emitted X-ray photons should be high enough to be detected [26].

A CN-6000 atomic force microscope (AFM) was used to provide high resolution images of the samples. This is a useful technique as 3-D images could be obtained and the roughness of films could be studied. Tapping mode was used to maximise the tip-sample interactions.

# 7 Results and Discussions

## 7.1 Sputter-Coated Films

Measured using the VDP technique, the best sputter-coated sample had a sheet resistance of 302 $\Omega$/sq. This is comparable to the values reported in literature [18][27].

The optical transmittance results are shown in Figure 7. The absorption edge is at approximately 390 nm. The average transmittance across wavelengths from 400 nm to 900 nm is 88.7%. The wave-like shape of the curve beyond the absorption edge is due to the constructive and destructive interference of light from the air/film interface and the film/substrate interface (Fabry-Pérot effects). From this we can deduce that the film surface is very smooth.

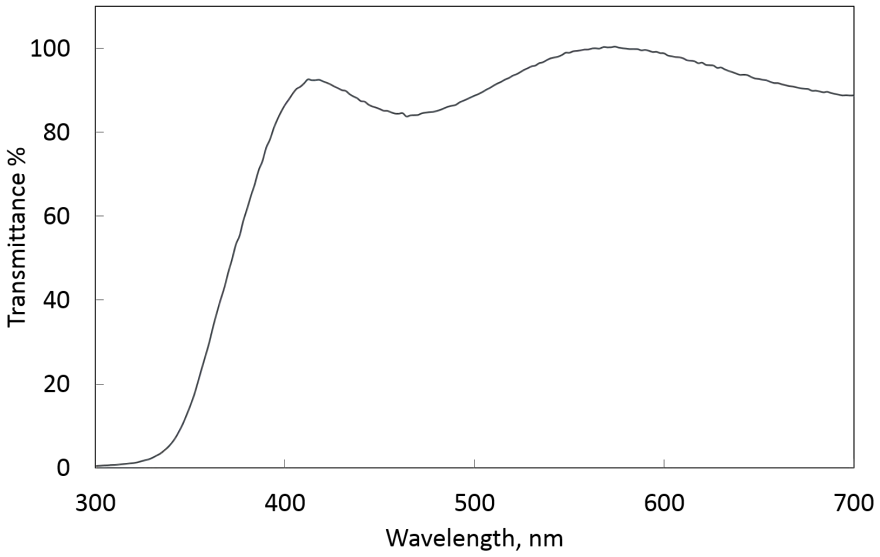


Figure 7: Transmission of a sputter-coated film.

An SEM image of the sputtered film is shown in Figure 8. The film surface is uniform and free of voids. The 3-D AFM image in Figure 9 shows the film's low roughness as the biggest feature size is only about 10 nm in height. For spin-coated films to achieve a reasonable conductivity, they too must exhibit uniform coverage and the absence of voids, as observed in the sputter-coated films.

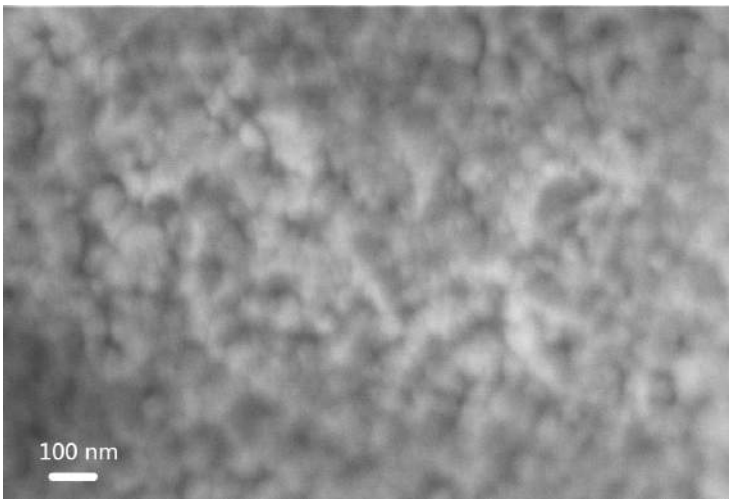


Figure 8: SEM image of a sputter-coated AZO film.

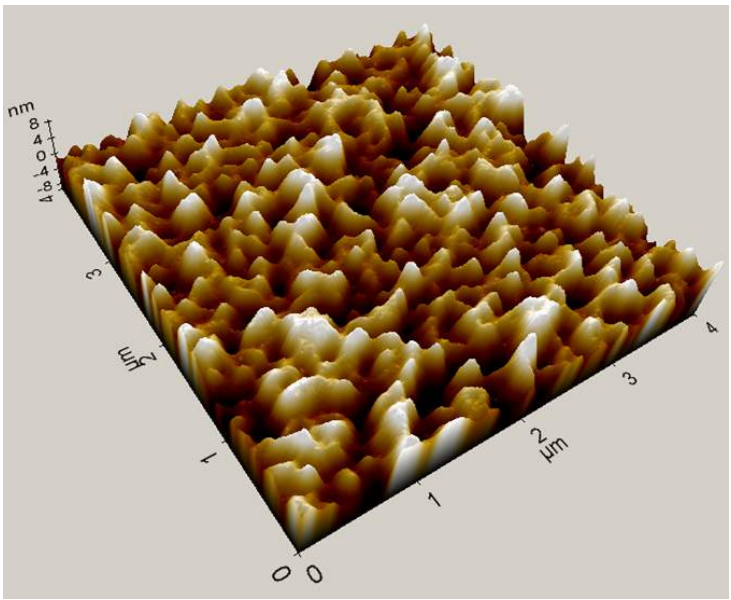


Figure 9: 3-D AFM image of a sputter-coated AZO film.

## 7.2 Spin-Coated Film Thickness

The thicknesses of the deposited thin films depend on a number of factors, namely, spin speed, spin duration and solution viscosity. The last factor is in turn determined by so-

lution concentration and evaporation rate of the base solution. Using the profilometer, it was shown that for the same spin duration, the film thickness, $d$, decreased with increasing spin speed, $\omega$. As exemplified in Figure 10, $d \propto \frac{1}{\sqrt{\omega}}$.

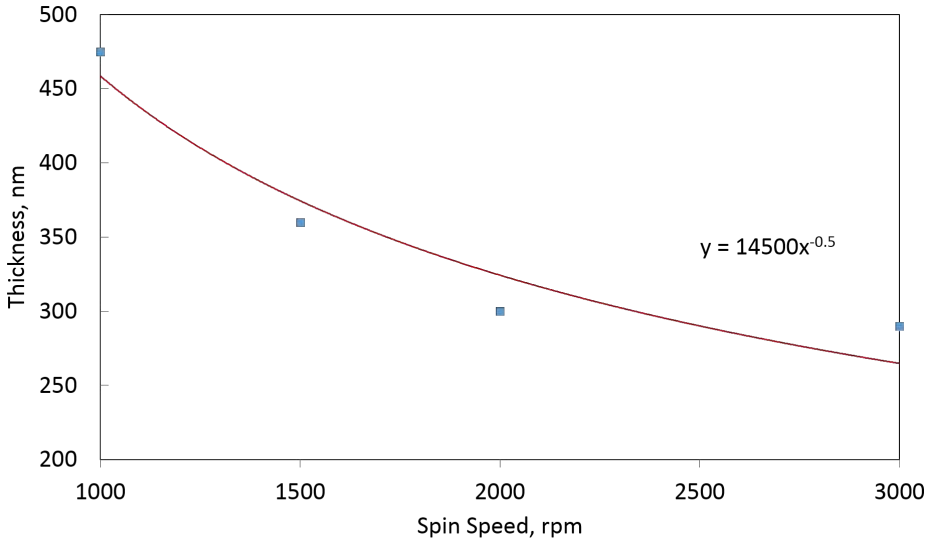


Figure 10: The dependence of film thicknesses on spin speeds for a 3 M water-based AZO solution spun for 30 s. The blue squares represent experimental results while the red line is the line of best fit, showing $d \propto \frac{1}{\sqrt{\omega}}$ dependency.

Initially, the spin-coat parameters were investigated using the purchased water-based AZO nanoparticle solution. Solution concentrations were varied from 0.75 M to 3 M. However, the relationship between film thickness and solution concentration was not clear from experimental results. This could be caused by the differences in the effective concentration of the AZO solutions deposited on the substrates, due to precipitation and inadequate dispersal of nanoparticles. From literature, it has been shown that thickness should be directly proportional to the solution concentration [28] [29] [30]. As the synthesised solutions all had a concentration of 0.3 M, a spin speed of 2000 rpm was chosen to give a film thickness of approximately 30 nm.

## 7.3 Base Solution and Quality of Films

The base solution was shown to make a significant difference to the quality of the films. Films coated by the water-based solution had many voids and a high surface roughness, as shown by the 3-D AFM image in Figure 11.

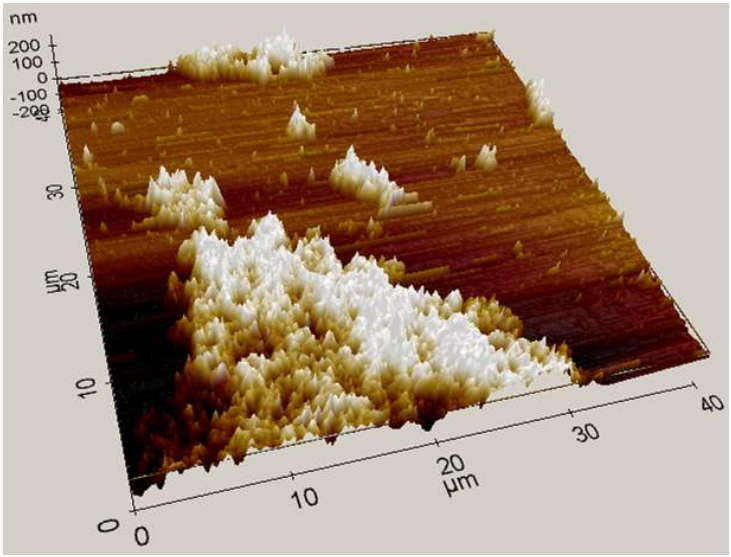


Figure 11: AFM image of an AZO film coated by the water-based solution.

These films were highly resistive and had sheet resistances in the order of $10^{12}\,\Omega$/sq. It is likely that the presence of voids disrupted the electrical current path and increased the sheet resistances in these films. In contrast, the ethanol-based solution synthesised in-house produced much more uniform coatings with very few voids. Their sheet resistances were in the order of $10^{8}\,\Omega$/sq, while all other parameters, such as film thicknesses and annealing temperature, were kept the same. Figure 12 and 13 show the surface differences between the films under a microscope.

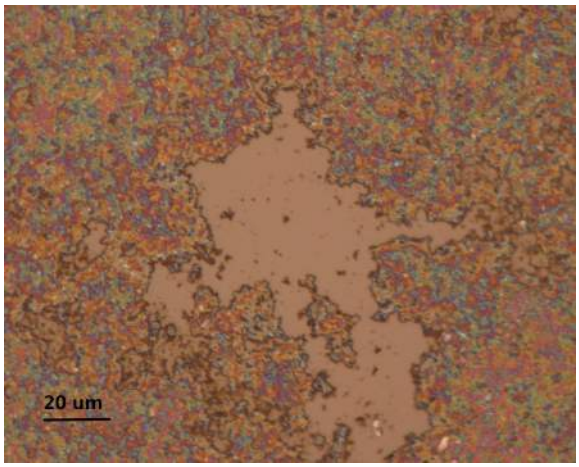


Figure 12: Microscope image of a film coated with the water-based solution.

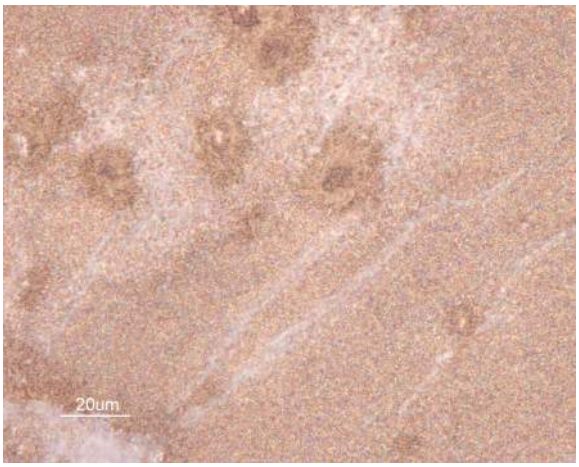


Figure 13: Microscope image of a film coated with the ethanol-based solution.

SEM images also revealed significant differences in terms of the surface morphology of the films, as shown in Figure 14 and 15. Films coated with one layer of the water-based solution displayed a granular morphology with considerable variations in their average surface roughness due to the agglomeration of nanoparticles. The film was neither dense nor compact, as seen from the relatively large areas with an absence of nanoparticles. The size of nanoparticles in the water-based solutions was only 15 nm [31] while the size of nanoparticles in the ethanol-based solutions ranged from 20 nm to 40 nm, as determined by the zetasizer and also observed from the SEM images. The larger particle size may have aided the gelation process, enabling the films to become more compact.

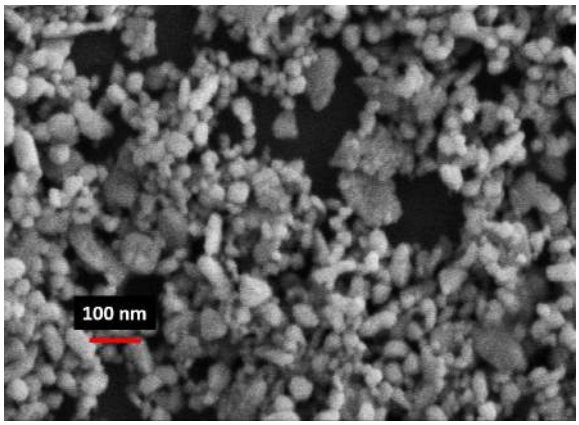


Figure 14: SEM image of a film coated with the water-based solution.

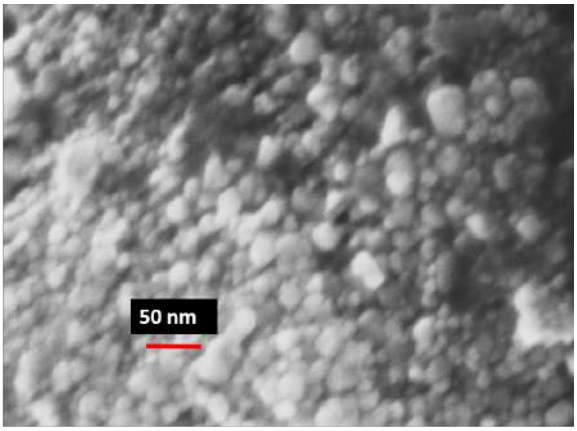


Figure 15: SEM image of a film coated with the ethanol-based solution.

One possible explanation on the decrease in voids is that the viscosity of the base solution can have a major impact on the quality of the films [32]. Solutions with lower viscosities tend to create the issue of the film drying before a uniform wet-layer has been produced. This induces swirls and voids in the film. Water has a lower viscosity of 0.894 mPa s than ethanol's 1.074 mPa s [33]. Also, as zinc acetate is much more soluble in ethanol than in water, it is likely that the ethanol-based solution is more homogeneous to begin with. To conclude, as the viscosity of the liquid and the solubility of the precursors in that liquid play important roles in determining the film quality, ethanol is more suitable than water as a base solution for AZO solution synthesis.

## 7.4 Aluminium Precursors

In terms of electrical conductivity, the films made by solutions with $Al(NO_3)_3$ as the precursor performed better than those with $AlCl_3$ as the precursor. The results are shown in Figure 16. As for optical transmittance, $AlCl_3$ showed slightly better results, as shown in Figure 17.

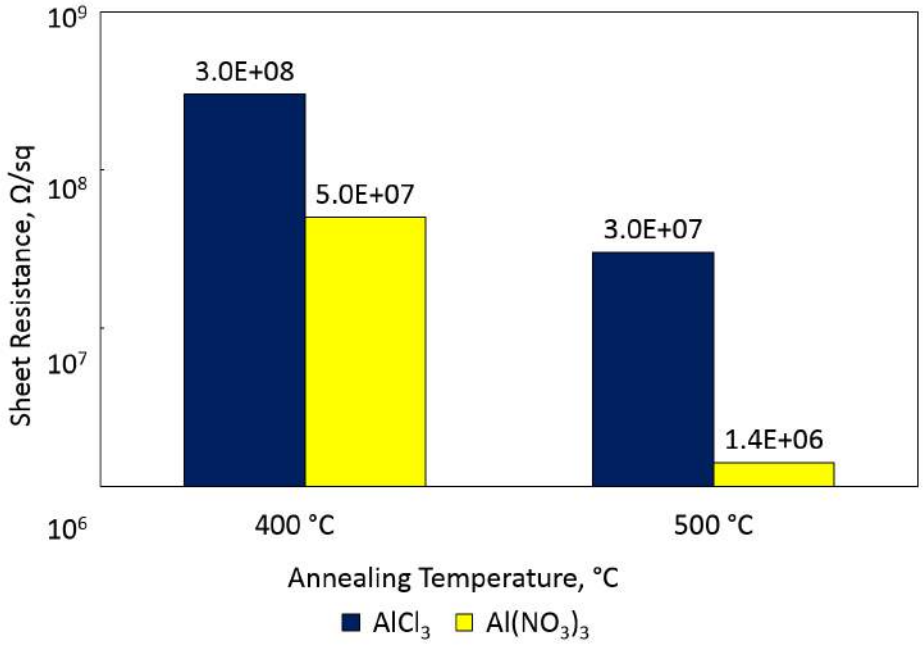


Figure 16: Sheet resistances of the films prepared from solutions synthesised using zinc acetate and two different aluminium precursors. The graph also shows a preliminary trend that an increasing annealing temperature decreases the sheet resistances. This will be discussed in detail in later sections.

This is evident that the starting chemicals used for the synthesis of AZO nanoparticles have a strong influence on the important properties of the films. It has been shown in other papers that the precursors used can in fact influence the shape and size of nanoparticles [6]. The reason may be that different anions have different properties and are selectively absorbed on the surface of crystal faces. This changes the surface energy distribution and affects the growth behavior of these crystals faces, thus impacting on the morphology of the films. The later samples were all made from solutions with $Al(NO_3)_3$ as the dopant precursor. It was chosen because of the lower resistance value obtained from the films and also its lower material cost.

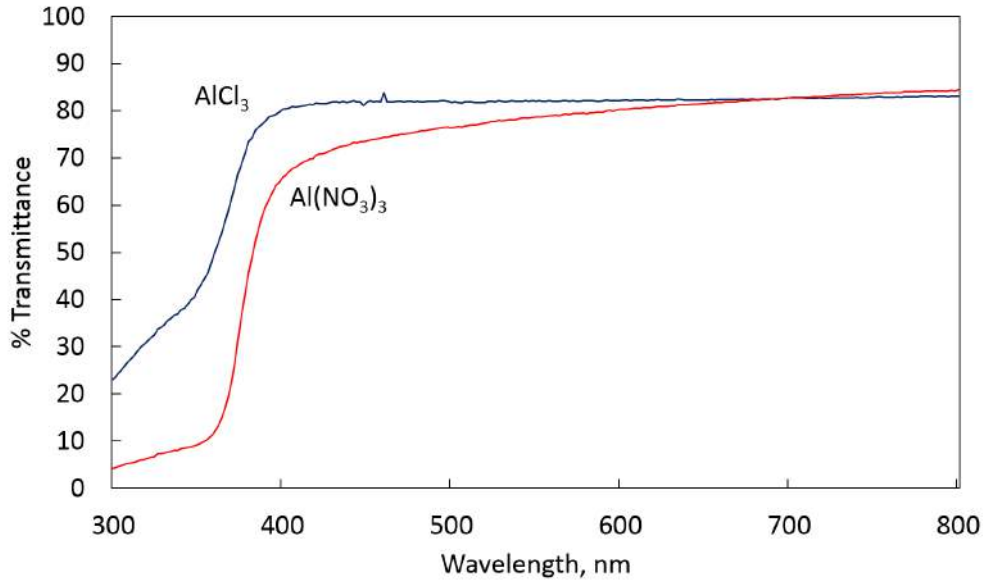


Figure 17: Optical transmittance of of films prepared from solutions synthesised using zinc acetate and two different aluminium precursors.

## 7.5 Multi-layer Coating

In order to produce films that are free of voids and cracks, more than one layer of coating is usually needed. In the literature, it is consistently agreed that multi-layer coating improves film properties [34][35], but the effect on the multi-layer coating of AZO has not been extensively researched. Optimum number of layers that have been mentioned in papers ranged from one to ten [36][37][38]. However, it is difficult to compare results across the papers since the optimum number of layers to coat should depend on the solution concentration, which is a parameter often not explicitly stated in papers. As detailed below, the experimental results obtained in this project led to the conclusion that the optimum number of layers when coating with a 0.3 M AZO solution is three.

### 7.5.1 Optical Properties

In this project, it was discovered that the film thickness is directly proportional to the number of layers coated, as each layer has approximately the same thickness. Despite the increased film thicknesses, optical transmittance of the films was only marginally affected. All films coated with one to six layers were able to achieve an average transmittance of above 85% over the wavelength range of 400 nm to 900 nm. This suggests

that the transmission losses are caused by reflection, and the absorption in the films is minimal, as expected for a wide bandgap material.

### 7.5.2 Electrical Properties

The sheet resistance indeed depends on the number of layers coated. Compared to a one-layer film, the sheet resistance of a two-layer film decreased by more than one order of magnitude, as shown in Figure 18. The initial decrease in resistivity is non-

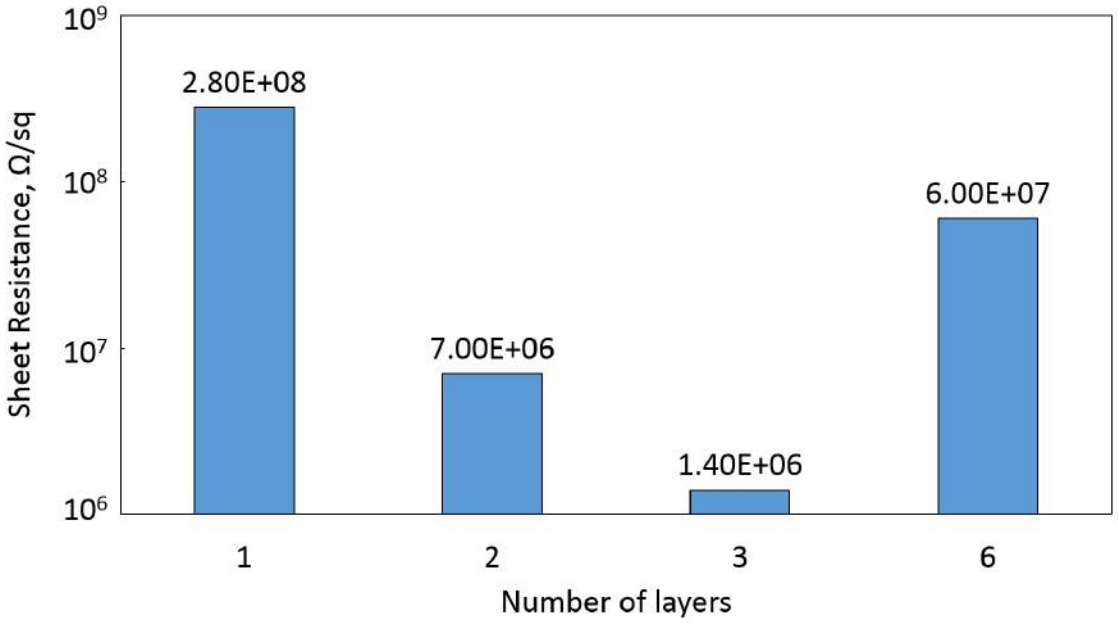


Figure 18: Variation of sheet resistance with the number of layers coated.

linear. This presumably occurs because after a second layer is coated, voids are filled up by additional nanoparticles, hence greatly improving the film quality. Carrier density might also increase slightly with more coatings, as suggested by Schuler *et al.*[38].

Beyond three layers, the repeated heating and drying between coatings may have caused more cracks in the film due to the mismatch in the extent of thermal expansion between layers.

### 7.5.3 Film Morphology

A fairly different morphology was obtained in multi-layer coatings made of thin individual layers, as seen in Figure 19 and 20. The grain size of the three-layer film was much bigger than the grain size of the one-layer film. The bigger grain size should

have contributed to the higher electrical conductivity, as electron scattering at grain boundaries is reduced.

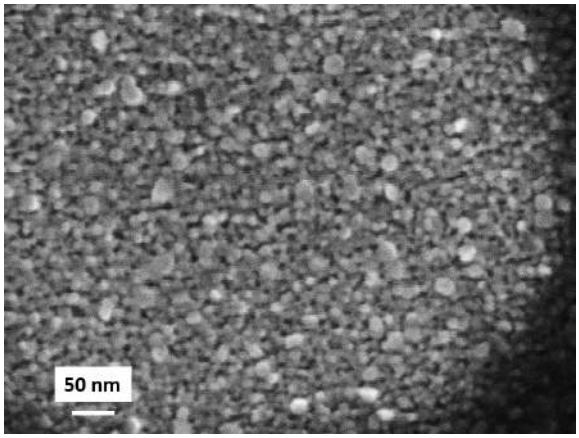


Figure 19: SEM image of a film coated with one layer of 1 wt% doped AZO.

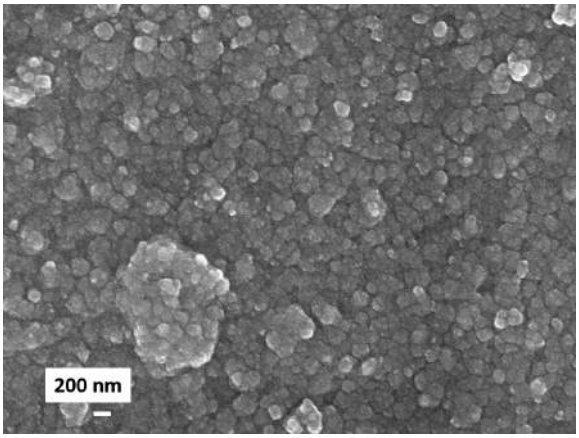


Figure 20: SEM image of a film coated with three layers of the same solution.

As discovered in some papers by performing transmission electron microscopy (TEM) on film cross-sections, a columnar growth can take place in multi-layer films, instead of an agglomeration of spherical particles as in single-layer films [38][39][40]. A schematic of the columnar growth process in multi-layer films is shown in Figure 21. The randomly orientated crystallites of the first layer may have served as nuclei for the columns. This columnar growth increases the grain size perpendicular to the surface. Compared to aggregates of nearly spherical nanoparticles, this columnar structure may have enhanced the carrier mobility due to a higher mean free path and a lower surface scattering of the electrons.

Therefore, besides the elimination of voids on films and the increased grain size in lateral direction, columnar growth may be a further contributing factor to the increase in electrical conductivity observed from the multi-layer films. The presence of columnar growth could not be verified for films made in this project as performing TEM is beyond the scope of this project.

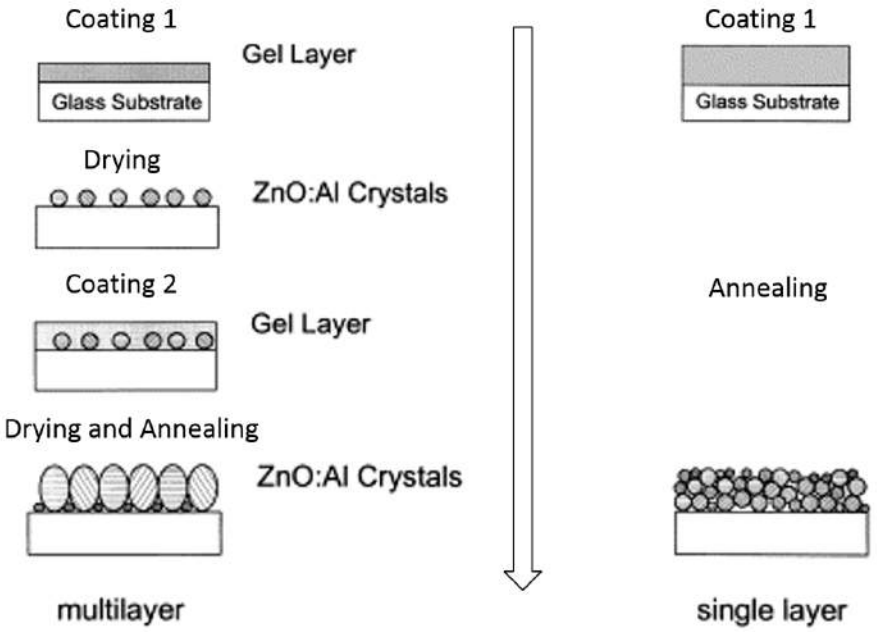


Figure 21: A schematic of the crystal growth observed in single and multi-layer sol-gel AZO films. Multi-layer coating leads to columnar crystal growth while single layer results in randomly oriented spherical crystals. Source: Modified from Figure 11 of [38].

## 7.6 Drying Process between Layers of Coating

The purpose of drying between the layers of coating is to evaporate the solvent and remove organic residue before a new layer is spun on. It is distinguished from the annealing process, which is a period of prolonged heating after all layers have been spun on. Drying is usually carried out at a lower temperature and for a much shorter duration compared to annealing. Two parameters that must be considered are the drying duration and the drying temperature [21][41].

### 7.6.1 Drying Duration

If the drying duration is too short, the homogeneity of films will be compromised because the second layer is being spun onto a partially-wet first layer. In this project, a drying duration of two minutes was deemed sufficient to evaporate off the excess solvent, since ethanol only has a boiling point of 78.4 °C. This is shorter than the drying time of ten minutes described in many papers [41] [36] [42], as the solvent used in those papers is 2-methoxyethanol, which has a higher boiling point of 125 °C.

### 7.6.2 Drying Temperature

As for drying temperature, an overly low temperature results in incomplete drying. For this project, the drying temperature was varied at 100 °C, 200 °C and 300 °C. Keeping all other parameters constant, drying the films at a temperature of 300 °C produced films with the lowest sheet resistances. This agrees well with the recommendations made in papers [42][41].

An interesting phenomenon discovered in some films is the presence of a dendritic morphology on film surface, as shown in Figure 22. The possible cause is that after the last layer is coated, the sample is directly placed on the 500 °C hotplate for annealing, skipping the drying step. This sudden increase in temperature may have caused dendritic nucleation. Since this phenomenon was not systematically studied, its effect on film properties is unclear.

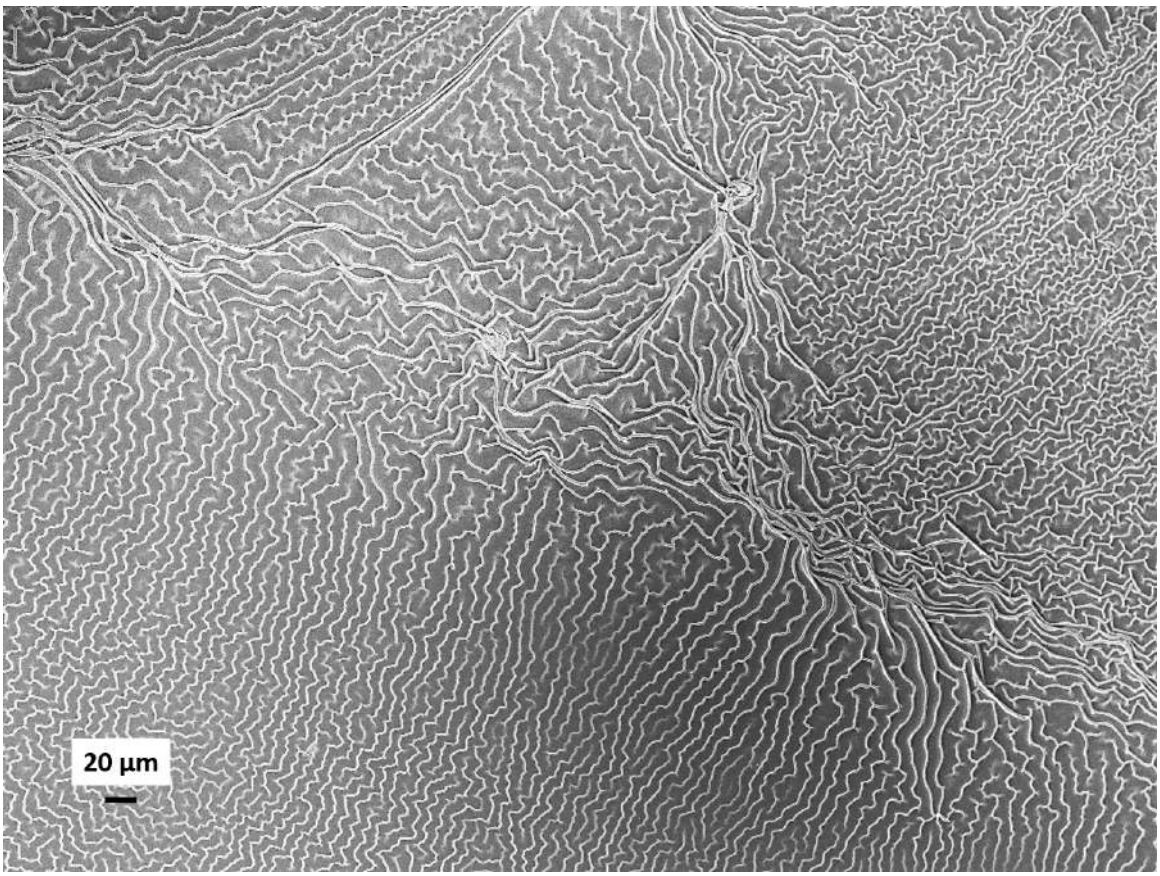


(a)

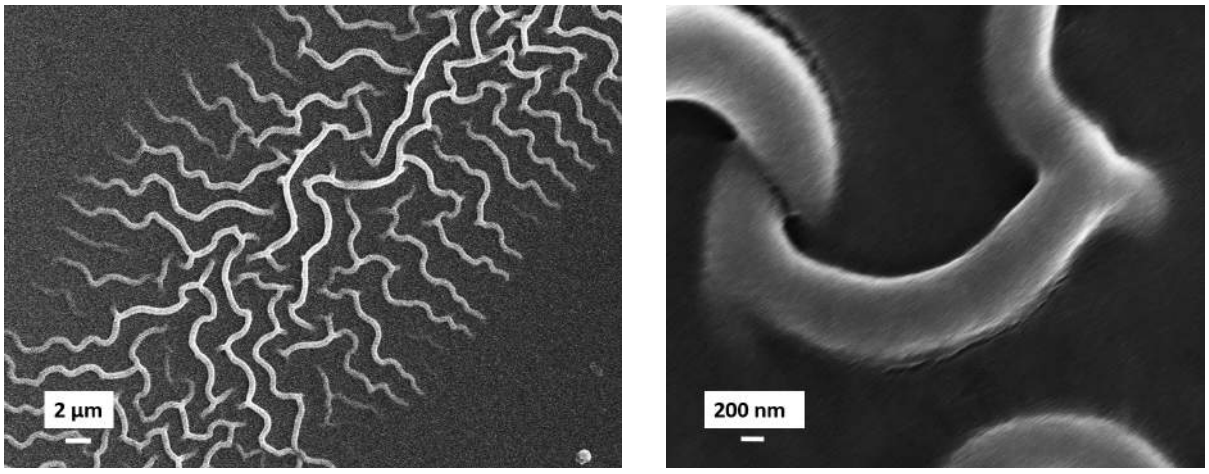


(b) (c)

Figure 22: Dendrites observed with different magnifications using the SEM.

## 7.7 Varying Doping Concentrations

Due to the reasons mentioned in the previous sections, all samples analysed from this section onwards were coated with three layers, with a drying temperature of 300 °C and a drying time of two minutes.

### 7.7.1 EDX Characterisation

The incorporation of Al was confirmed by performing elemental analysis using EDX. Figure 23 shows the EDX spectrum and elemental composition of a film coated with 1 wt% doped AZO. The atomic percentages are rounded up to whole numbers since the measuring system had a $\pm 1\%$ uncertainty in atomic percentage values. The detected silicon and calcium atoms come from the glass substrates [43]. This is an expected occurrence as the penetration depth of EDX is in the micrometer range. The detected zinc and oxygen species have a stoichiometric ratio of close to one, which corresponds to the ratio of a ZnO compound. The extra oxygen atoms detected should also be from the substrate.

For subsequent measurements, there seemed to be a systematic error present in the EDX system such that there were always more aluminium atoms detected than likely. Therefore, firm conclusions about the stoichiometry of the film could not be made. Nevertheless, relative comparison of EDX results between samples exhibited the expected trend according to their nominal doping levels [44].

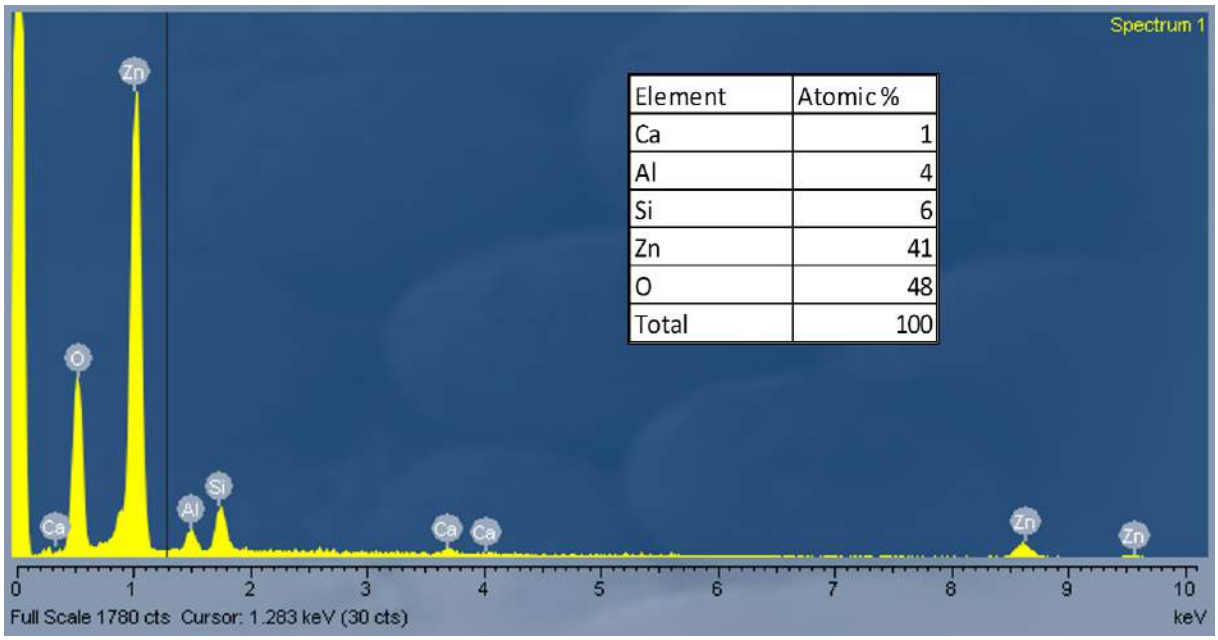


Figure 23: EDX results of a sample coated by 1 wt% doped AZO solution.

### 7.7.2 Electrical Properties

The sheet resistance generally decreased with an increasing doping concentration, until it reached a minimum at a 1 wt% doping. It then increased as doping level increased to 2 wt%. A small discrepancy was that 0.5 wt% films gave higher or comparable resistances to 0.25 wt% films, under all annealing conditions. This could be due to a systematic error as these films were made in two different laboratories and were annealed on two different hot plates (due to the unanticipated closure of original laboratory). The trends are shown in Figure 24.

The nominally undoped ZnO conducted electricity poorly, probably due to the low concentration of mobile charge carriers. As doping increases, extra electrons contributed by the Al atoms result in a higher carrier concentration. This will increase conductivity as $\sigma = ne\mu$, where $\sigma$ is the electrical conductivity, $n$ is the electron concentration in n-type semiconductor and $e$ is the electronic charge. However, as the doping level becomes excessive, electron scattering from ionised impurities becomes more dominant. The average path that an electron can travel before being scattered decreases, therefore electrical conductivity starts to drop. In this project, AZO's optimum doping level was found to be 1 wt%.

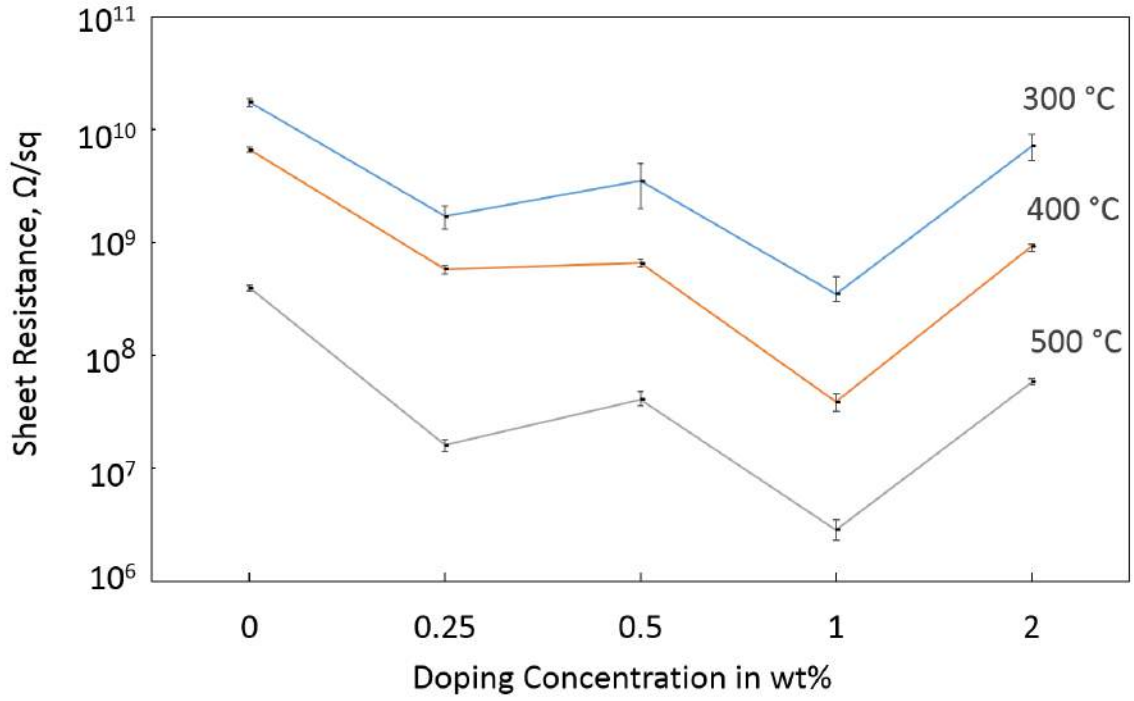


Figure 24: Average sheet resistance is at its minimum at a 1 wt% doping level. The error bars show the highest and lowest reading for samples made under that particular condition.

### 7.7.3 Optical Properties

Doping level did not seem to affect the average transmittance of the films, as all films showed an average transmittance of 85% to 90% across the wavelength range of 400 nm to 900 nm. Interestingly, the absorption edge shifted to a shorter wavelength with increased doping, as shown in Figure 25. A shorter wavelength corresponds to a greater photon energy and implies a greater apparent bandgap. This phenomenon is known as blueshift.

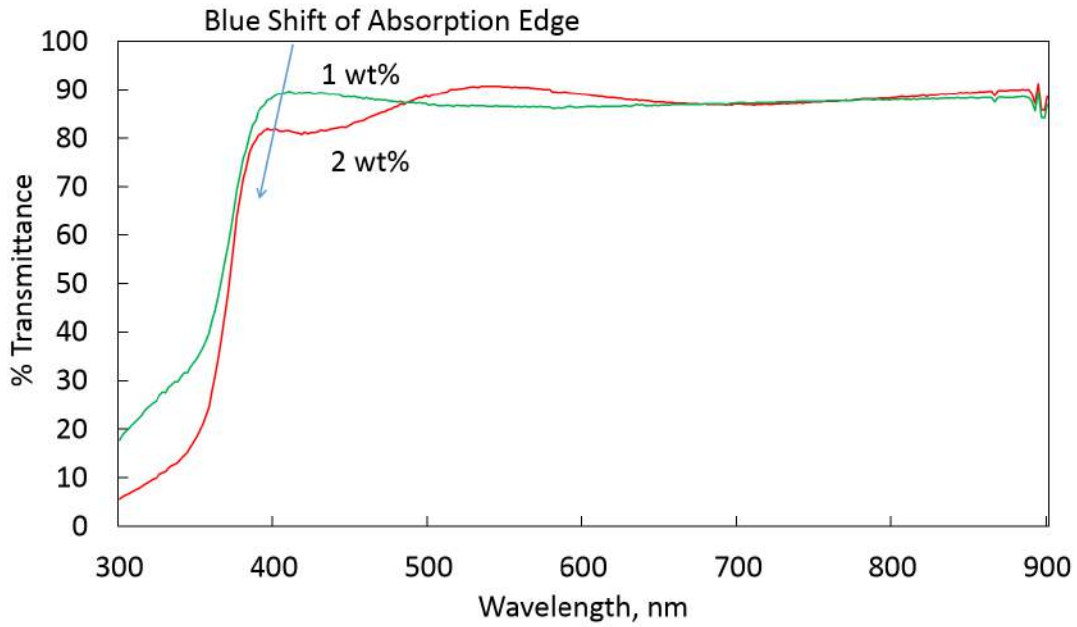


Figure 25: Blueshift of absorption edge with increased doping.

Next, Tauc gaps of the AZO films were deduced from their transmittance spectra. The Tauc gap is the apparent bandgap of a semiconductor material. It is an especially useful means of characterising materials that are not perfectly crystalline, as is the case for AZO. For a direct bandgap material, the Tauc gap can be determined by using the following relation: $(\alpha h\nu)^2 = c(h\nu - E_g)$, where $\alpha$ is the absorption coefficient, $c$ is a constant, $h$ is Planck's constant, $\nu$ is the frequency of light, and $E_g$ is the Tauc gap to be determined. $(\alpha h\nu)^2$ is plotted against $h\nu$ and a best fit line is plotted for the linear part of the curve. The extrapolated x-intercept is the Tauc gap of the material.

The absorption coefficient, $\alpha$, was calculated from the equation $\frac{\ln(\frac{1}{T})}{d}$, where $T$ is the transmittance value at a particular wavelength and $d$ is the film thickness. As mentioned earlier, for a 0.3 M AZO solution, the thickness of one layer of film was about 30 nm when spun at 2000 rpm. As all the films analysed here have three layers of coating, the thickness was nominally taken to be 100 nm for all films. This was also confirmed by imaging the film cross-sections using the SEM. All films used for the calculation of Tauc gap were made under the same conditions. The only difference between them is the doping level of the starting solution, which does not affect film thicknesses.

Tauc plots showing the Tauc gaps for films made from undoped ZnO and 2 wt% doped AZO are shown in Figure 26. Tauc gap was found to increase with increasing doping levels. A summary of Tauc gaps for all doping levels is shown in Figure 27.

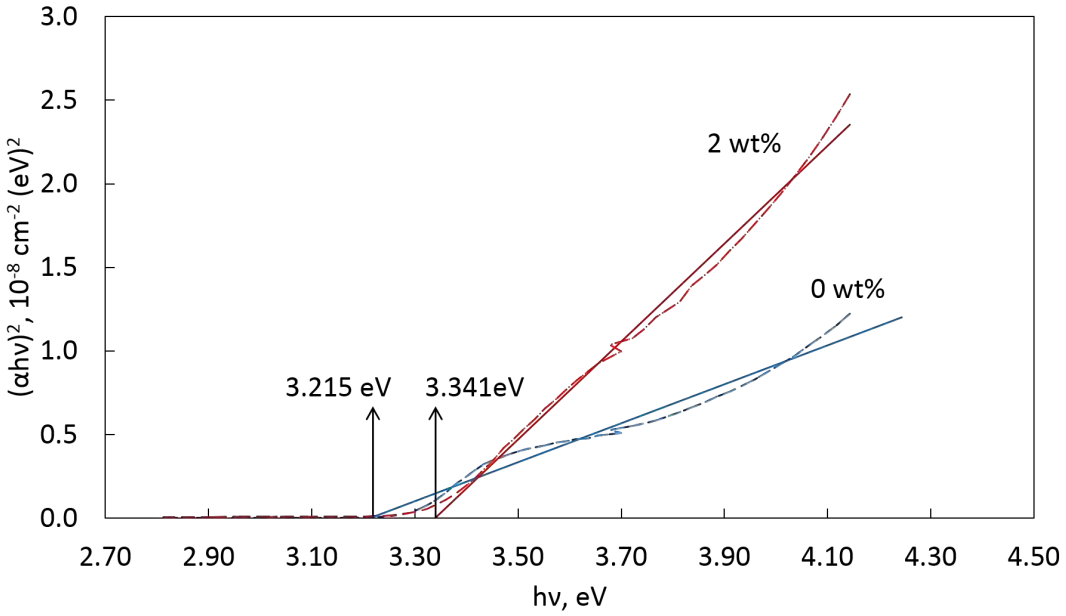


Figure 26: Tauc plots showing the Tauc gaps for an undoped film and a 2 wt% doped film. The dotted lines are the raw data lines. The solid lines are the linear best fit lines.

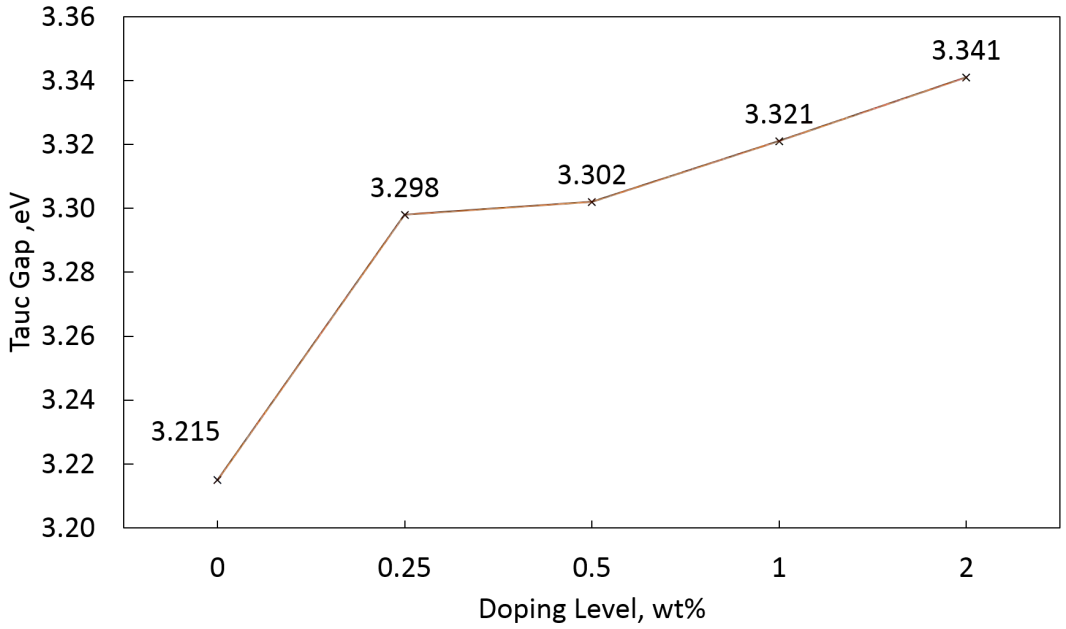


Figure 27: The Tauc gap increased with doping concentrations. The line is only a guide for the eyes.

The widening of apparent bandgaps can be explained by the Burstein-Moss theory. For nominally doped semiconductors, the Fermi level lies between the conduction band minimum and valence band maximum. However, in a semiconductor where degenerate doping occurs, its Fermi level is pushed into the conduction band so the lowest states in the conduction band become occupied by electrons. Hence, valence electrons require extra energy to be excited to the higher, unoccupied energy states in the conduction band. This leads to a widening of the optically observed bandgap, and provides evidence that the ZnO has indeed been doped with aluminium. While the exact values of the Tauc gap depend heavily on the detailed sol-gel fabrication conditions, the values obtained in this project agree well with many papers for films fabricated using similarly doped solutions [45] [46].

## 7.8 Varying Annealing Temperature

### 7.8.1 Morphology

With an increasing annealing temperature, the surface morphology of the films exhibited a notable transformation, as seen in Figure 28 and 29. At an annealing temperature of 300 °C, the film surface consisted of fine grains. The average grain size was only about 15 nm. As annealing temperature increased to 500 °C, the grains became larger and more densely packed. The grain size was approximately thrice as before. The increase in crystallite size has consistently been highlighted as the main reason behind the improvement of film properties with an increasing annealing temperature [40][42].

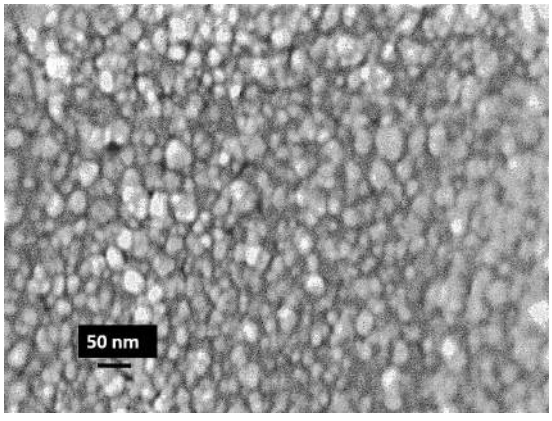


Figure 28: SEM image of a film annealed at 300 °C for 60 minutes.

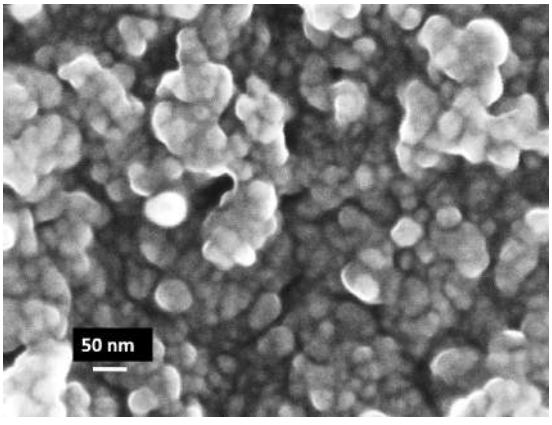


Figure 29: SEM image of a film annealed at 500 °C for the same duration.

### 7.8.2 Electrical Properties

Sheet resistances of the films decreased significantly with increasing annealing temperatures, as shown in Figure 30. This is because high temperature annealing helps to eliminate defects in crystals so the crystallinity of films improves. Also, the size of crystallites increases so electron scattering at grain boundaries reduces. This in turn enhance the mobility of the charge carriers. The improvement in crystallinity has been further confirmed in many papers by performing X-ray diffraction (XRD) analysis [42][47].

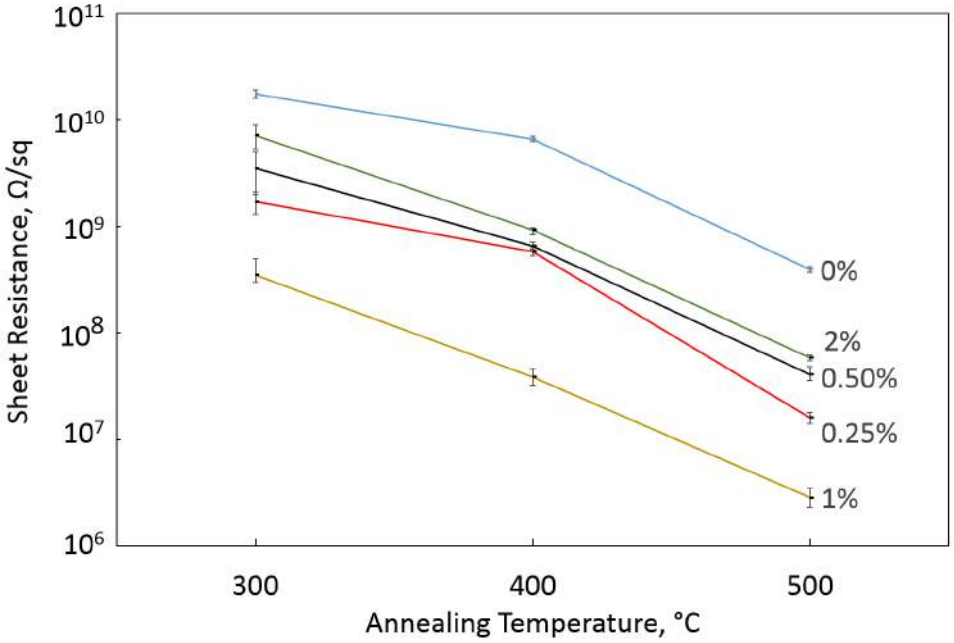


Figure 30: Dependence of the average sheet resistance on annealing temperature, for different doping concentrations in wt %. Error bars show the highest and lowest reading for samples made under that particular condition.

### 7.8.3 Optical Properties

The optical transmittance of the films increased with increasing annealing temperatures, as shown in Figure 31. This could also be attributed to the increased crystal size, which lowers the amount of optical scattering at grain boundaries.

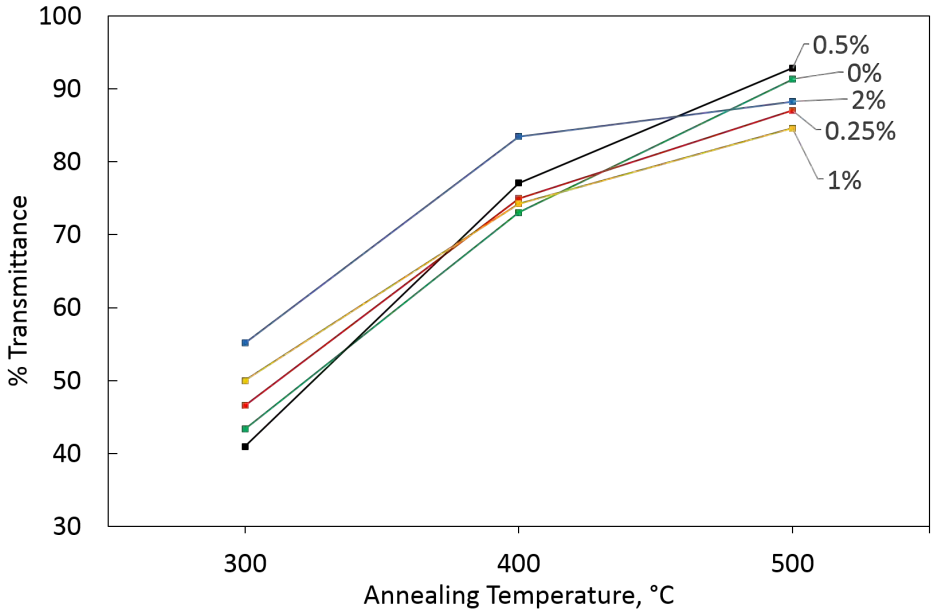


Figure 31: Dependence of the average transmittance over wavelength range of 400 nm to 900 nm on annealing temperature, for different doping concentrations in wt %.

## 7.9 Varying Annealing Duration

The annealing duration was varied at 30, 60 and 90 minutes while keeping the annealing temperature at 500 °C. This did not have a significant effect on the sheet resistance and the optical transmittance of the films. It could be due to the relatively high annealing temperature used, which makes 30 minutes of annealing sufficient. Similar conclusions have been made in literature, where annealing duration had a much more pronounced effect on films annealed at 300 °C than those annealed at 400 °C [48].

## 7.10 Coating AZO on Graphene

A layer of 1 wt% doped AZO solution was coated onto a graphene film of one atomic layer thick. The objective of this experiment was to test if electrical conductivity of the graphene film would improve with the AZO coating. The spin speed was 2000 rpm and the spin time was 30 s. The film was then annealed at 200 °C for 60 minutes. A comparatively low annealing temperature was chosen to avoid the chemical degradation of graphene. This is because many papers have stated observations that using an annealing temperature above 350 °C risks graphene-substrate interaction, which degrades electron mobility in graphene [49][50].

The sheet resistance of the graphene film was 900 Ω/sq before AZO coating. However, this value increased to 3900 Ω after the coating. This could be attributed to the mechanical degradation of the graphene layer due to the spinning motion. Perhaps a much lower spin speed should be used to give a more favourable resistance value. This could not be further investigated due to the lack of graphene samples. The transmittance could not be measured with the UV-visible spectrometer as graphene film was on an opaque substrate.

## 7.11 MWCNT/AZO Composite Thin Films

Multi-wall carbon nanotubes (MWCNTs) are formed by concentrically nested, and turbostratically aligned graphene cylinders, as shown in Figure 32. They are chemically and mechanically robust and are particularly well-suited to form composites with metal oxides in solutions [51]. They have been reported to enhance the conductivity of the ZnO film while not compromising on its optical transmittance [51][52].

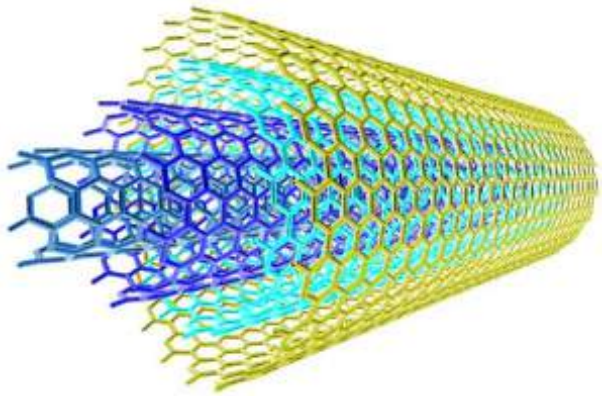

Figure 32: A 3-D model of the structure of MWCNT. Source:imgarcade.com

In this project, MWCNT of an unknown concentration in distilled water was added to a 0.25 wt% doped AZO solution in ethanol. Three different volumes of MWCNT solution were added to portions of the AZO solution such that the volume of MWCNT : AZO were of the ratio 1:1, 2:1 and 5:1 respectively. The three mixtures were sonicated for ten minutes before being spun onto the glass substrates. As before, three layers were spun on with a drying temperature of 300 °C and a drying time of two minutes between layers. The films were then annealed at 500 °C for 60 minutes.

Theoretically, high densities of MWCNTs must be incorporated to reach an acceptably low electrical resistance. But the trade off is that as more MWCNTs are introduced, the optical transparency will degrade due to the increased absorption cross-section. Unfortunately, this trend was not obvious in the experimental results obtained. The transmittance values of the films were all in the range of 85% to 90%. Also, the sheet resistances only improved marginally for films coated by two of the three mixtures. A summary is shown in Table 2.

| **Coating Solution** | **Sheet Resistance (MΩ/sq)** | **Transmittance (%)** |
|---|---|---|
| 0.25 wt% AZO | 16 | 87.1 |
| MWCNT:AZO 1:1 | 23 | 85.4 |
| MWCNT:AZO 2:1 | 11 | 88.0 |
| MWCNT:AZO 5:1 | 9 | 86.9 |

Table 2: Properties of the films coated with a 0.25 wt% AZO solution and three different AZO/MWCNT mixtures.

The reason could be that the MWCNT solution was too dilute, so that there were not enough CNTs to reach percolation. This is confirmed by the SEM image as shown in Figure 33. Also, the mixing of distilled water and ethanol may have required a longer drying time between layers.

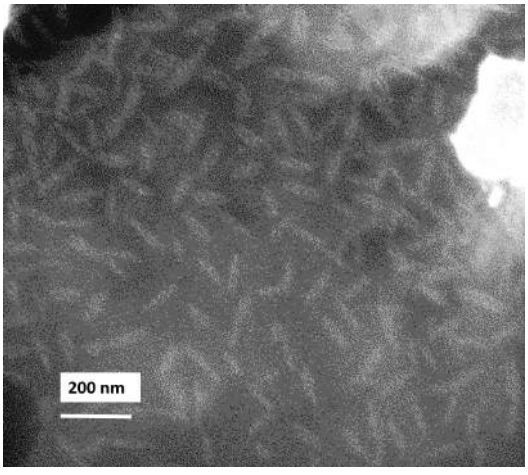


Figure 33: SEM image of a film coated by an MWCNT/AZO solution mixture with a volumetric ratio 5:1. The grey and elongated shapes are the CNTs.

Attempts were made to quantify the amount of carbon incorporated into the films by using EDX. This was unsuccessful as the energies of the X-ray emitted from electron transitions in an element is proportional to the square of its atomic number. Due to carbon's small atomic number of six, its emitted X-ray may be too weak to be detected, or that sensitivity to it is too low [26]. Also, EDX usually has a detection limit of 0.1 wt% to 2 wt%, depending on the element of interest [53]. Hence if the carbon content in the scan area is less than the detection threshold, its presence may not be picked up.

# 8 Figure of Merit

Figure of merits (FOM) are useful tools for comparing the performance of TCO thin films between different materials and deposition techniques, using the sheet resistance and optical transmittance of the films. While many FOMs have been suggested in literature, this project chose the FOM developed by Haccke [54] as it has been much more commonly cited in papers on the fabrication of thin films. For this FOM, $\phi = \frac{T^{10}}{R_s}$, where $T$ is the optical transmittance and $R_s$ is the sheet resistance. A high FOM implies a good optical transmittance and a small sheet resistance, hence a better quality film. Table 3 shows a comparison between the films synthesised in this project and a commercial ITO film with a mid-range performance. While sputter-coated AZO films achieved an FOM comparable to the ITO film, the spin-coated AZO films still need significant improvements on their electrical conductivity.

| Film type | Rs ($\Omega$/sq) | Transmittance (%) | FOM ($\times 10^{-6}\,\Omega^{-1}$) |
|---|---|---|---|
| Sputter-coated AZO | $3.02 \times 10^2$ | 92.0 | 1440 |
| Best spin-coated AZO | $1.03 \times 10^6$ | 92.0 | 0.422 |
| MWCNT/AZO | $9.00 \times 10^6$ | 86.9 | 0.027 |
| Commercial ITO on glass [2] | $1.50 \times 10^2$ | 85.0 | 1970 |

Table 3: Comparison of FOMs among different films.

This FOM, though very useful in comparing the technical performances of different films, does not take into account the price of raw materials and the complexity of deposition technique. If those factors are taken into consideration, spin-coated AZO film can still be desirable in certain applications, even though it does not display a very high electrical conductivity at the moment. Distinct advantages of the sol-gel process,

combined with AZO's excellent optical properties, could still make AZO attractive in optical applications such as in photonics [55].

# 9 Future Improvements

The lowest sheet resistance obtained in this project was in the low MΩ/sq range. Though this value is considerably far from the research goal stated in Section 4.2, it is comparable to many spin-coated films made under similar conditions, as published in some papers [36][42][56]. In addition, the optical transmittance obtained was well above the target. This section will discuss a few possible ways to further improve the electrical conductivity of the spin-coated films.

Due to the unavailability of equipment, one parameter that was not investigated in this project was the annealing environment. This could hold the key to a significant decrease in the sheet resistance of the spin-coated films. Annealing in vacuum environment, in pure argon gas, in pure nitrogen gas and in forming gas (a mixture of nitrogen and hydrogen gas) have all been reported to improve AZO film properties to various extents [36][56]. Annealing at temperatures above 500 °C could also be carried out to investigate whether the improvement in film performance brought by higher annealing temperatures reaches a plateau above a certain temperature.

Another important factor to consider is the pre-deposition treatment of the substrates. Some have reported an improvement on film conductivity by thoroughly cleaning the substrate with dilute acid [20]. Pre-heating of substrate could also be done to investigate whether this improves film quality.

Compared to sputter-coating, spin-coating is a much more manual process that involves a large number of parameters, of which some could be equipment-dependent. This results in poor reproducibility of high quality films. Though many AZO films were fabricated using a set of closely matching parameters, a wide range of sheet resistances have been reported in literature [57]. A way to solve this problem is to automate the spin-coating process as much as possible. This could be done by using spin-coaters installed with an auto-dispenser. Such a measure would ensure that the amount of

solution deposited and the way solutions are deposited stay consistent across all samples, therefore improving the reproducibility of high quality films. Another potentially beneficial technique is to dispense the solution dynamically, i.e dispensing the solution onto a spinning substrate.

In terms of improving the coating solution, the MWCNT/AZO idea could be further developed by mixing a more concentrated, ethanol-based MWCNT dispersion with the synthesised AZO solution. To fully exploit the flexibility of the sol-gel technique, other dopants or substances that may improve the electrical conductivity of the films could also be added to the AZO solution. For example, it has been reported that adding ultra-pure water has shown to considerably improve the conductivity of dip-coated AZO films [17].

An additional characterisation technique that would be very useful is Hall effect measurement. This requires a magnetic field to be set up perpendicular to the sample surface while electrical current is passed across the surface. By measuring the Hall voltage, the carrier concentration and carrier mobility can be determined. As electrical conductivity depends on these two factors, knowing them will help to better pinpoint the necessary modifications needed to further improve the sol-gel technique.

# 10 Conclusion

This project investigated the parameters involved in producing AZO thin films via sol-gel technique. The sheet resistance and the optical transmittance of the films were used as performance indicators in making comparisons amongst various films made under different conditions. The key findings include:

- Water is not a suitable base for the spin-coating technique. Ethanol is a better option.
- Compared to $AlCl_3$, $Al(NO_3)_3$ is a more effective precursor in making AZO solutions as films exhibited lower sheet resistances.
- Multi-layer coatings can help to improve film quality up to a certain extent. For an AZO solution concentration of 0.3 M, the optimum number of layers is found

to be three.

- Drying duration and temperature are two very important parameters that influence the quality of multi-layer films.
- Doping ZnO with aluminium significantly improves the electrical conductivity of the films. However, beyond a doping level of 1 wt%, the conductivity starts to decrease, most probably due to a drop in carrier mobility.
- Higher annealing temperatures improve film quality appreciably.
- Above 30 minutes, annealing duration does not have a noticeable effect on the film performance.

Sputter-coated AZO films made in this project showed excellent properties that can rival the commercial ITO films. This shows that as a material, AZO has the potential to replace ITO, especially when the latter becomes prohibitively expensive due to the scarcity of indium. However, much research is still needed in developing a solution-processable technique for depositing AZO films. As discussed earlier and also in literature, very similar experimental procedures can produce films with hugely different properties. In order to make the sol-gel technique sufficiently reliable and repeatable, it is essential to automate the fabrication process as much as possible, even at the research stage.

# 11 Bibliography

# References

[1] G. Hautier, A. Miglio, G. Ceder, G.-M. Rignanese, and X. Gonze, "Identification and design principles of low hole effective mass p-type transparent conducting oxides," *Nature Communications*, vol. 4, Aug. 2013.

[2] "ITO Glass, Xumatic. Inc." `http://www.xumatic.com/index.php?route=product/category&path=25_31`. Accessed: 9 May 2015.

[3] "TCO choices for CIGS manufacturing." `http://blogs.indium.com/blog/indium-corporation-2/tco-choices-for-cigs-manufacturing`. Accessed: 2015-05-23.

[4] D. Lison, "Sintered indium-tin-oxide (ITO) particles: A new pneumotoxic entity," *Toxicological Sciences*, vol. 108, pp. 472–481, Apr. 2009.

[5] "Supply Of The iPhone's Touch Sensitive Coating Is Running Out." http://www.cultofmac.com/235537/supply-of-the-iphones-touch-sensitive-coating-is-running-out/. Accessed: 9 May 2015.

[6] A. Alkahlout, "Synthesis and characterization of aluminum doped zinc oxide nanostructures via hydrothermal route," *Journal of Materials*, vol. 2014, Mar. 2014.

[7] D. Ginley, H. Hosono, and D. C. Paine, *Handbook of Transparent Conductors*. Springer Science & Business Media, Sept. 2010.

[8] S. Pearton, *GaN and ZnO-based Materials and Devices*. Springer Science & Business Media, Jan. 2012.

[9] T. Minami, "Transparent conducting oxide semiconductors for transparent electrodes," *Semiconductor Science and Technology*, vol. 20, p. S35, Apr. 2005.

[10] P. P. Sahay and R. K. Nath, "Al-doped zinc oxide thin films for liquid petroleum gas (LPG) sensors," *Sensors and Actuators B: Chemical*, vol. 133, pp. 222–227, July 2008.

[11] S. H. Jeong, B. N. Park, S. B. Lee, and J. H. Boo, "Metal-doped ZnO thin films: Synthesis and characterizations," *Surface and Coatings Technology*, vol. 201, pp. 5318–5322, Feb. 2007.

[12] S. Hofmann, "CUED 4C3 lecture notes: Thin Flim Technology," Nov. 2014.

[13] G. Rampf and R. McCafferty, "Devising an APC strategy for metal sputtering using residual gas analyzers," *Micro Magazine*, Feb. 2007.

[14] T. Minami, H. Nanto, and S. Takata, "Highly Conductive and Transparent Aluminum Doped Zinc Oxide Thin Films Prepared by RF Magnetron Sputtering," *Japanese Journal of Applied Physics*, vol. 23, p. L280, May 1984.

[15] "Spin Coaters, Information." http://www.globalspec.com/learnmore/manufacturing_process_equipment/surface_coating_protection/spin_

coaters. Accessed: 18 May 2015.

[16] "Wet coating technologies for glass." http://www.solgel.com/articles/Nov00/mennig.htm. Accessed: 18 May 2015.

[17] J. B. Nehmann, N. Ehrmann, R. Reineke-Koch, and D. W. Bahnemann, "Aluminum-doped zinc oxide sol-gel thin films: Influence of the sol's water content on the resistivity," *Thin Solid Films*, vol. 556, Apr. 2014.

[18] M. J. Alam and D. C. Cameron, "Preparation and properties of transparent conductive aluminum-doped zinc oxide thin films by solgel process," *Journal of Vacuum Science & Technology A*, vol. 19, pp. 1642–1646, July 2001.

[19] J. D. Wright and N. A. J. M. Sommerdijk, "The Future," in *Sol-Gel Materials: Chemistry and Applications*, vol. 8, CRC Press, Dec. 2000.

[20] S. Salam, "Solgel synthesis of intrinsic and aluminum-doped zinc oxide thin films as transparent conducting oxides for thin film solar cells," *Thin Solid Films*, vol. 529, pp. 242–247, Feb. 2013.

[21] V. Musat, B. Teixeira, E. Fortunato, R. C. C. Monteiro, and P. Vilarinho, "Al-doped ZnO thin films by solgel method," *Surface and Coatings Technology*, vol. 180181, pp. 659–662, Mar. 2004.

[22] "WHO | Quality assurance." http://www.who.int/medicines/areas/quality_safety/quality_assurance/en/. Accessed: 9 May 2015.

[23] "Sigma-Aldrich Product Catalogue." https://www.sigmaaldrich.com/catalog/product. Accessed: 2015-01-07.

[24] V. Tvarozek, P. Sutta, S. Flickyngerova, I. Novotny, P. Gaspierik, M. Netrvalova, and E. Vavrinsky, "Preparation of Transparent Conductive AZO Thin Films for Solar Cells," in *Semiconductor Technologies* (J. Grym, ed.), InTech, Apr. 2010.

[25] "Keithley", "Keithley Application Note Series Four-Probe Resistivity and Hall Voltage Measurements with the Model 4200-SCS," Jul. 2011.

[26] "Energy-dispersive X-ray (EDX) spectroscopy." http://cime.epfl.ch/EDX. Accessed: 2015-05-23.

[27] X. C. Ma, "Influence of hydrogen annealing on structure and optoelectronic properties in al doped ZnO thin films," *Material Technology*, vol. 29, no. 2, pp. 101–104, Mar. 2014.

[28] "Spin Coating Theory." `http://www.brewerscience.com/research/processing-theory/spin-coating-theory#process-theory`. Accessed: 2015-05-05.

[29] T. Schneller, R. Waser, M. Kosec, and D. Payne, *Chemical Solution Deposition of Functional Oxide Thin Films*. Springer Science & Business Media, Jan. 2014.

[30] F. Bensebaa, *Nanoparticle Technologies: From Lab to Market*. Academic Press, Dec. 2012.

[31] "AZO Nanoparticles / AZO Nanopowder Water Dispersion (AZO, 15nm, 20wt%)." `http://www.us-nano.com/inc/sdetail/3799`. Accessed: 2015-05-25.

[32] "Spin coating: a guide to theory and techniques." `http://www.ossila.com/pages/spin-coating`. Accessed: 2015-01-12.

[33] R. C. Weast, *CRC Handbook of Chemistry and Physics: A Ready-reference Book of Chemical and Physical Data*. CRC Press, 1982.

[34] Bressanone, "Presentations on coatings." `http://www.chimica.unipd.it/offerte/pubblica/dottorato/coatings.pdf`, Sept. 2006.

[35] J. H. Prosser, T. Brugarolas, S. Lee, A. J. Nolte, and D. Lee, "Avoiding Cracks in Nanoparticle Films," *Nano Letters*, vol. 12, no. 10, pp. 5287–5291, Sep. 2012.

[36] V. Kondratiev, I. Kink, and A. Romanov, "Low Temperature Sol-Gel Technique for Processing Al-Doped Zinc Oxide Films," *Materials Physics and Mechanics*, vol. 17, pp. 38–46, June 2013.

[37] M. Jun, S. Park, and J. Koh, "Comparative studies of Al-doped ZnO and Ga-doped ZnO transparent conducting oxide thin films," *Nanoscale Research Letters*, vol. 7, p. 639, Nov. 2012.

[38] T. Schuler and M. A. Aegerter, "Optical, electrical and structural properties of sol gel ZnO:Al coatings," *Thin Solid Films*, vol. 351, pp. 125–131, Aug. 1999.

[39] C. Goebbert and G. Gasparro, "Influence of the Layer Morphology on the Electrical Properties of Sol Gel Transparent Conducting Oxide Coatings," vol. 19, no. 1, pp. 435–439, 2000.

[40] S. Kuo, W. Chen, and F. Lai, "Effects of doping concentration and annealing temperature on properties of highly-oriented Al-doped ZnO films," *Journal of Crystal Growth*, vol. 287, pp. 78–84, Jan. 2006.

[41] S. S. Shariffudin, M. H. Mamat, S. H. Herman, and M. Rusop, "Influence of Drying Temperature on the Structural, Optical, and Electrical Properties of Layer-by-Layer ZnO Nanoparticles Seeded Catalyst," *Journal of Nanomaterials*, vol. 2012, p. e359103, Nov. 2012.

[42] M. Gao and Zhang, "Effect of Annealing Conditions on Properties of Sol-Gel Derived Al-Doped ZnO Thin Films," *Chinese Physics Letter*, vol. 26, no. 8, pp. 366–369, Aug. 2009.

[43] "Chemistry of Glass," *Corning Museum of Glass*, Dec. 2011.

[44] A. B. Rosli, M. M. Marbie, S. H. Herman, and M. H. Ani, "Gold-Catalyzed Growth of Aluminium-Doped Zinc Oxide Nanorods by Sputtering Method," *Journal of Nanomaterials*, vol. 2014, p. e672047, July 2014.

[45] T. Minami, H. Nanto, and S. Takata, "Optical properties of aluminum doped zinc oxide thin films prepared by RF magnetron sputtering," *Japanese Journal of Applied Physics*, vol. 24, no. 8, p. L605, Aug. 1985.

[46] C. Benouis, A. Sanchez-Juarez, and M. Aida, "Physics Properties Comparison Between Undoped ZnO and AZO, IZO Doped Thin Films Prepared By Spray Pyrolysis," *Journal of Applied Sciences*, vol. 7, pp. 220–225, Feb. 2007.

[47] L. Huang, N. Ren, B. Li, and M. Zhou, "Effect of Annealing on the Morphology, Structure and Photoelectric Properties of AZO/Pt/FTO Trilayer Films," *Acta Metallurgica Sinica (English Letters)*, vol. 28, pp. 281–288, Jan. 2015.

[48] S. Lee, Y. Park, D. Kim, D. Baek, J. Yi, B. Hong, W. Choi, and J. Lee, "Thermal stability of hydrogen-doped AZO thin films for photovoltaic applications," *Materials Research Bulletin*, vol. 58, pp. 126–131, Oct. 2014.

[49] A. Eftekhari and P. Jafarkhani, "Curly Graphene with Specious Interlayers Displaying Superior Capacity for Hydrogen Storage," *The Journal of Physical Chemistry C*, vol. 117, pp. 25845–25851, Dec. 2013.

[50] V. Skakalova and A. B. Kaiser, *Graphene: Properties, Preparation, Characterisation and Devices*. Elsevier, Feb. 2014.

[51] S. Kim, S. Choi, C. Park, and H. Jin, "Transparent conductive ITO thin films through the sol-gel process using metal salts," *Thin Solid Films*, vol. 347, pp. 155–160, June 1999.

[52] I. Y. Bu and M. T. Cole, "A highly conductive and transparent solution processed AZO/MWCNT nanocomposite," *Ceramics International*, vol. 40, pp. 1099–1104, Jan. 2014.

[53] "The basic theory of quantitative analysis and corrections | SEM School." `http://emu.uct.ac.za/training/sem-school/basic-theory-of-edx-quantitative-analysis-correction/`. Accessed: 2015-05-23.

[54] G. Haacke, "New figure of merit for transparent conductors," *Journal of Applied Physics*, vol. 47, no. 9, Sep. 1976.

[55] L. Znaidi, T. Touam, D. Vrel, N. Souded, S. B. Yahia, O. Brinza, A. Fischer, and A. Boudrioua, "AZO Thin Films by Sol-Gel Process for Integrated Optics," *Coatings*, vol. 3, pp. 126–139, July 2013.

[56] Y.-h. Ho, Y. Chen, and C. Wu, "Effect of Annealing Ambient on the Electrical and Optical Properties of Aluminum-Doped ZnO Films Produced via a Sol-Gel Process," *Journal of Electronic Materials*, vol. 43, pp. 2644–2650, Mar. 2014.

[57] L. Znaidi, "Sol-gel deposited ZnO thin films: A review," *Materials Science and Engineering: B*, vol. 174, pp. 18–30, Oct. 2010.

# 12 Appendix

## 12.1 Risk Assessment Retrospective

This project required a a large amount of experimental work, hence risk assessments were thoroughly conducted before undertaking any procedures in the lab. Induction tours were attended before starting experimental work in any new facility. In order to better understand the risks involved in working with chemicals, a 3-hour chemical safety course was attended. COSHH forms were completed before the purchase of aluminium chloride and aluminium nitrate.

Risk assessments were conducted again when experimental work was shifted to Nanoscience Centre's wet lab, after the CAPE chemistry lab was shut down. This was necessary as different working environments may impose different risks and have different emergency response procedures.

In conclusion, the risk assessments done at various stages of this project sufficiently eliminated any foreseeable risks.